



Synthesis, biological evaluation and *in silico* modeling of novel pan-genotypic NS5A inhibitors

Andrey A. Ivashchenko^{a,b,c}, Yan A. Ivanenkov^{b,e,*}, Vladimir A. Aladinskiy^c, Ruben N. Karapetian^a, Angela G. Koryakova^a, Alexey A. Ryakhovskiy^a, Oleg D. Mitkin^a, Dmitry V. Kravchenko^a, Nikolai P. Savchuk^{a,d}, Bogdan A. Zagribelnyy^c, Alexander V. Ivashchenko^{a,b,d}

^a Chemical Diversity Research Institute, Rabochaya St. 2a, Khimki, Moscow Region 141401, Russia

^b ChemDiv, 6605 Nancy Ridge Drive San Diego, CA 92121, United States

^c Moscow Institute of Physics and Technology (State University), 9 Institutskiy lane, Dolgoprudny City, Moscow Region 141700, Russia

^d Avisa Pharmaceuticals LLC, 1835 E. Hallandale Beach Blvd, #442, Hallandale Beach, FL 33009, United States

^e Institute of Biochemistry and Genetics Russian Academy of Science (IBG RAS) Ufa Scientific Centre, Ufa, Russia

ARTICLE INFO

Keywords:

NS5A inhibitors
HCV
Medicinal chemistry
In silico modeling
Combinatorial synthesis

ABSTRACT

A series of novel small-molecule pan-genotypic hepatitis C virus (HCV) NS5A inhibitors with picomolar activity containing 2-[(2S)-pyrrolidin-2-yl]-5-[4-(4-{2-[(2S)-pyrrolidin-2-yl]-1H-imidazol-5-yl}buta-1,3-diyn-1-yl)phenyl]-1H-imidazole core was designed based on molecular modeling study and SAR analysis. The constructed *in silico* model and docking study provide a deep insight into the binding mode of this type of NS5A inhibitors. Based on the predicted binding interface we have prioritized the most crucial diversity points responsible for improving antiviral activity. The synthesized molecules were tested in a cell-based assay, and compound **1.12** showed an EC₅₀ value in the range of 2.9–34 pM against six genotypes of NS5A HCV, including gT3a, and demonstrated favorable pharmacokinetic profile in rats. This lead compound can be considered as an attractive candidate for further clinical evaluation.

1. Introduction

Hepatitis C infection caused by hepatitis C virus (HCV)^{1,2} is one of the most common liver diseases and is widespread throughout the world. HCV infection is of growing international concern due to its substantial effect on morbidity and mortality. A leading cause of cirrhosis, hepatocellular carcinoma (HCC), liver transplantation, and liver-related death worldwide, the HCV-related disease burden continues to increase as the infected population advances to late stage liver disease. The disease inflicts an immense health and economic burden on countries due to the infection's hepatic and extrahepatic effects. The 2015 global prevalence estimate of 71.1 million people have hepatitis C infection.³ In 2016, approximately most 399 000 people died of hepatitis C, mostly from cirrhosis and hepatocellular carcinoma (primary liver cancer). HCV causes both acute and chronic infection. New HCV infections are usually asymptomatic. Some persons get acute hepatitis which does not lead to a life-threatening disease. Around 30% (15–45%) of infected persons spontaneously clear the virus within 6 months of infection without any treatment. The remaining 70% (55–85%) of persons will develop chronic HCV infection. Of those with

chronic HCV infection, the risk of cirrhosis ranges between 15% and 30% within 20 years.⁴

Until recently, HCV was classified into 8 distinct genotypes that differed by > 30% at the nucleotide level. Genotypes are further divided into subtypes with a sequence divergence of > 15%.⁴ To date, 86 confirmed HCV subtypes have been described.⁵ Genotypes 1, 2 and 3 are distributed worldwide, genotype 1 being the predominant one, specifically subtypes 1a and 1b.³ Genotype 1 is the best established treatment.⁶ Because of the large genetic diversity of genotype 2, often joining recombinants with other genotypes, there are some strains of genotype 2, more resistant to therapy.⁷ The most difficult in the treatment of genotype 3.^{8,9} Within the six major clinical HCV genotypes, genotype 3 represents 22–30% of all infection and is described as a unique entity with higher rates of steatosis, faster progression to cirrhosis, and higher rates of hepatocellular carcinoma.⁹

In recent years, unconditional success has been achieved in the combinatorial therapy of hepatitis C.^{6–11} One of the main components of the combinatorial therapy of HCV infection are nonstructural protein 5A (NS5A) inhibitors which displayed much higher potency in controlling HCV infection than other drugs. This is because NS5A exerts

* Corresponding author at: ChemDiv, 6605 Nancy Ridge Drive San Diego, CA 92121, United States.

E-mail address: yai@chemdiv.com (Y.A. Ivanenkov).

<https://doi.org/10.1016/j.bmc.2020.115716>

Received 11 February 2020; Received in revised form 7 August 2020; Accepted 16 August 2020

Available online 20 August 2020

0968-0896/ © 2020 Published by Elsevier Ltd.

Abbreviations

HCV	Hepatitis C Virus	uronium	
NS5A	Nonstructural protein 5A (HCV)	DIPEA	Diisopropylethylamine
SAR	Structure-Activity Relationship	MeCN	Acetonitrile
EC ₅₀	Half-maximal effective concentration	EtOAc	Ethyl acetate
gT3a	Genotype 3a (HCV)	Val	Valine
HCC	Hepatocellular carcinoma	Ph	Phenyl
FDA	Food and Drug Administration	Gly	Glycine
gT1b	Genotype 1b (HCV)	gT1a	Genotype 1a (HCV)
SM	Structural modifications	gT4a	Genotype 4a (HCV)
D -I	Domain I (NS5A)	gT5a	Genotype 5a (HCV)
MD	Molecular dynamics	Huh7	Hepatoma cell line
RMSF	Root mean square fluctuation	PK	Pharmacokinetics
RMSD	Root mean square deviation	PO	Per-oral route of administration
Trp	Tryptophan	AUC	Area under curve
PPI	Protein-Protein Interaction	AUC _{INF}	Area under curve (infinite time)
NS4B	Nonstructural protein 4B (HCV)	AUC _{last}	Area under curve (the last point)
RAV	Resistance Associated Variant	C _{max}	Maximal plasma concentration
R	Arginine (except R ¹ and R ² – radicals)	T _{max}	The time take to reach C _{max}
A	Alanine	T _{1/2}	Half-life time
Y	Tyrosine	MRT _{INF}	Mean residence time (infinite approximation)
Q	Glutamine	MRT _{last}	Mean residence time (the last time point)
S	Serine	F _{abs}	Absolute bioavailability
EC ₅₀	Half-maximal efficacy concentration	NMR	Nuclear magnetic resonance
T	Threonine	HPLC	High-performance liquid chromatography
P	Proline	UV	Ultra Violet irradiation
Moc	Methoxycarbonyl group	HRMS	High Resolution Mass Spectrometry
gT2a	Genotype 2a (HCV)	ESI	Electrospray Ionization
C	Cysteine	TEA	Triethylamine
BB	Building block	DCM	Dichloromethane
BDD	Buta-1,3-diyne-1,4-diyl group	LC/MS	Liquid chromatography/ mass-spectroscopy
boc	<i>tert</i> -Butyloxycarbonyl group	DMSO- <i>d</i> ₆	Dimethyl sulfoxide (fully deuterated)
THF	Tetrahydrofuran	ESIHRMS	High resolution electrospray ionization mass spectrometry
DMF	<i>N,N</i> -dimethylformamide	FBS	Fetal Bovine Serum
Et ₃ N	Triethylamine	DMEM	Dulbecco's modified Eagle's medium
MeOH	Methanol	CC ₅₀	Half-maximal cytotoxic concentration
Pd(PPh ₃) ₄	Tetrakis(triphenylphosphine)palladium (0)	EDTA	Ethylenediaminetetraacetic Acid
HATU	Hexafluorophosphate azabenzotriazole tetramethyl	IV	Intravenous route of administration
		MS	Mass-spectroscopy
		UPLC	Ultra High-Performance Liquid Chromatography

functionally essential effects in regulation of viral replication, assembly and egress, it has been considered a drug target for antiviral therapeutic intervention.¹² The first among pan-genotypic NS5A inhibitors was Daclatasvir (BMS-790052),^{13–15} approved of FDA July 24, 2015. It was followed by Elbasvir, (MK-8742),¹⁶ Ledipasvir (GS-5885),¹⁷ AV-4025,¹⁸ Ombitasvir (ABT-267),¹⁹ Samatasvir,^{20,21} Ruzasvir (MK-8408)²² and others. The large and ever-growing diversity of HCV genotypes and their subtypes dictates the search for new pan-genetic inhibitors of NS5A HCV with improved characteristics, which is currently associated primarily with the structural modifications (SM) of known core structures. The powerful picomolar pan-genotype inhibitors MK-6169^{23,24} and Pibrentasvir (ABT-530)²⁵ (Fig. 1) are examples of this SM. They were obtained as a result of a SM of Elbasvir and Ombitasvir, respectively.

In this paper, we present the rational design of novel AV-4025¹⁸ derivatives with an improved inhibition potency against HCV genotypes, especially gT3a. Particularly, we have developed *in silico* model for prediction the target activity mainly focusing on substituents at the phenyl ring in the linker fragment (Fig. 1).

2. Results and discussion

The structure of the vast majority of small-molecule NS5A inhibitors contains a linker and two terminal “End Caps” with pre-defined stereo-

configuration²⁶ (Fig. 1).

2.1. *In Silico* modelling

Considering the last trends in the title area, side-chain modifications in the linker area may lead to an improved pan-genotypic covering and higher activity. For instance, Elbasvir by Merck & Co. (Fig. 1) was launched in 2016 for the oral treatment of chronic HCV infection in combination with grazoprevir. The compound showed picomolar inhibition potency against many HCV genotypes, including 3a. Although the predicted binding mode of Elbasvir was presented,²⁷ the detailed docking studies have not been published yet. This side-chain modification motivated us to develop a special *in silico* model of dimeric 3D target structure with an attached *N*-terminal α -helices of NS5A using homology morphing. The main focus was placed on genotype 3a due to its prevalence within the Russian Federation in contrast to other geographic areas. In order to reconstruct the *N*-terminal region of NS5A gt3a, we exploited the binding mode-II model of gt1b published by Nettles et al. as a template structure. The authors reported two distinct asymmetric binding modes of Daclatasvir. Both models were validated experimentally with a library of structural analogs of Daclatasvir and are consistent with the studies dedicated to investigating the mechanism of action of NS5A inhibitors. Moreover, in the recent bioinformatic analysis of gt1a and gt1b HCV protein sequences, it was stated

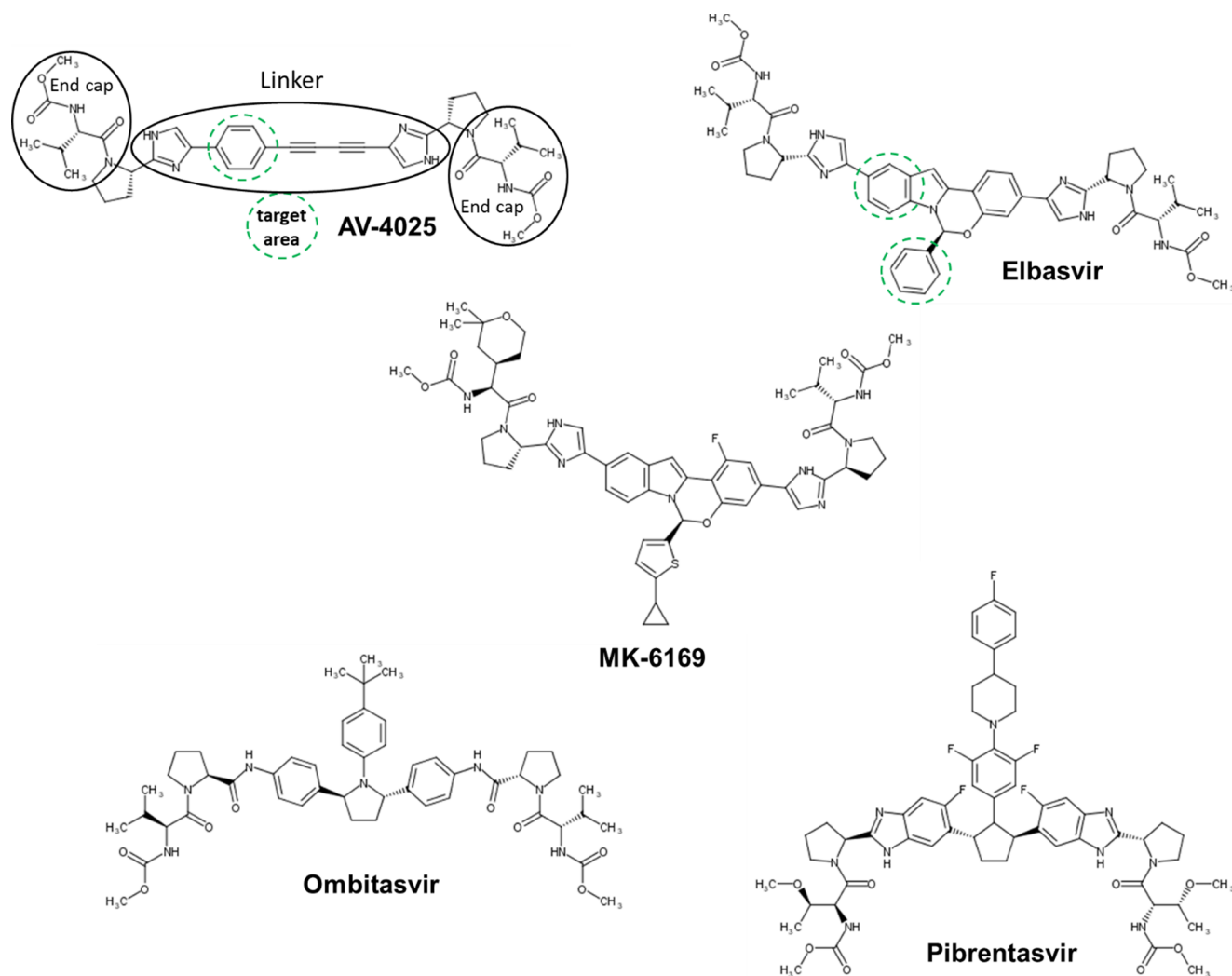


Fig. 1. Common topological pharmacophore model for NS5A inhibitors.

that the structural insights derived from the binding mode-II model agree with data on clinically relevant mutations of HCV.²⁸ In our previous work, we demonstrated that morphing Caps leads to inequivalent changes in antiviral potency.¹⁸ This fact also supports the hypothesis regarding asymmetric binding modes of NS5A inhibitors.

We used the homology modeling tool implemented in Maestro Schrödinger Software²⁹ to produce ten homology models. In order to evaluate the obtained 3D structures, we docked Elbasvir into all ten models and selected the model with the lowest energy score (Emodel of -115) for further steps. The Elbasvir predicted binding mode is represented in Fig. 2. The linker tightly occupied the cleft between D-I of the chain B and the AH of the chain A. B-R56 supposedly provided pi-cation interaction with indole of the tetracyclic scaffold. Interestingly, in our model, imidazole formed H-bond with a backbone carbonyl of G92 instead of the bridge with T95 as it was predicted for Daclatasvir, GSK-2336805, and GS-5885 in the model of gt1b.²⁷ The phenyl function was oriented towards the membrane and provided additional contacts with the α -helix. The model suggests that one of the peptide-like caps binds in the region of the flexible linker of chain B (Cap binding site I), forming a hydrogen bond between NH of A30 and carbonyl, while valine-carbamate moiety contacts P29, A30 and L31. Another End Cap occupied the binding site II, where both carbonyls of Pro-Val-carbamate were predicted to bind to two arginines A-R6 and B-R6 through H-bonds. Noteworthy, that NH of this Cap was directed at the hydroxyl of A-Y93 and possibly able to provide H-bond bridging.

We further investigated the amino-acid variants in the *N*-terminal α -helices and D-I of NS5A from HCV gT1b and gT3a to determine those which can be associated with the resistance to AV-4025 treatment (Fig. 3). To assess the significance of these variants, we aligned the known model of gt1b in complex with daclatasvir and our homology model of gt3a (Fig. 4). Among the first 100 residues, we highlighted the following key differences: (i) a side-chain of A-R30 was shown to provide strong hydrogen bond with carbamate moiety,²⁷ thus R30A variant results in loss of this interaction and can be considered as one of the vital RAV (Fig. 4A); (ii) T56R substitution in chain B may lead to steric clashes between a core structure and a bulky guanidinium moiety of B-R56 which is able to prevent tight fitting the cleft between D-I and AH consequently not allowing to appropriately place a peptide-like cap for H-bonding with B-Y93 (Fig. 4B); (iii) in our model we observe that the side chain of B-R6 is directed at the Cap binding site oppositely to gt1b (Fig. 4C), such orientation likely caused by two amino-acid replacements A-T56R and B-S3D. Indeed, the proximity of positively charged A-R56 may lead to the displacement of the B-R6 functional group while B-D3 stabilizes this orientation through electrostatic interactions and H-bond.

Interestingly, previously published models³⁰ have predicted, that Q54 of each monomer in gt1b forms a relatively strong H-bond with imidazole or pyrrolidino-carbonyl, hence Q54S substitution may attenuate activity. However, due to significant structural differences, the binding mode-II model by Nettles et al., as well as the gt3a model

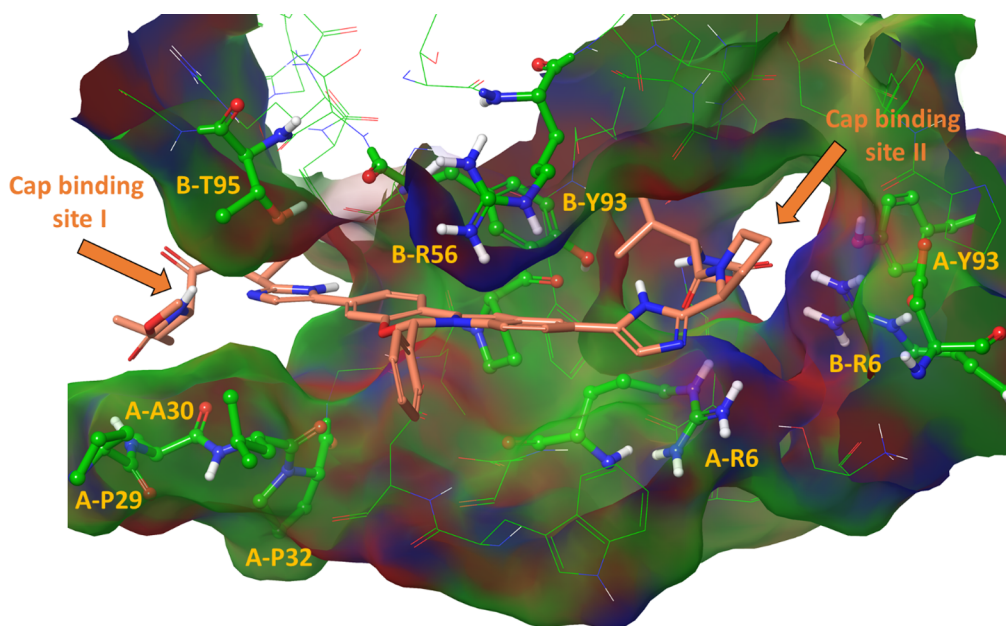


Fig. 2. The predicted binding mode of Elbasvir (orange) to NS5A gt3a. The protein structure is depicted as green. Compound and key residues are represented as a thick tube model. Orange arrows indicate the putative binding sites of End Caps.

described here, do not suggest such an interaction. Noteworthy, the presence of two arginine groups in the proximity of a binding site may cause electrostatic repulsion results in reducing the binding affinity. This hypothesis was comprehensively discussed in the study concerned with the structural insights into the binding modes of NS5A inhibitors.³⁰ The authors have suggested that resistance of gT1a Q30R mutant is likely explained by repulsion between R30 and R56. In accordance with our model of NS5A gT3a, the binding site contains four arginine residues A-R6, B-R6, A-R56, and B-R56. We also suggested that tight binding with NS5A can be affected by the proximity of these residues.

The built model was exploited to provide structural insight into the binding mode of AV-4025 in order to indicate the opportunities for improving the affinity towards NS5A gT3a. The putative binding mode of AV-4025 is depicted in Fig. 5. The diynyl-phenyl core was predicted to fit the groove formed by A-G33, A-P35, B-Y93, A-D10, and A-R-6. Imidazole ring distal to phenyl of the spacer was accommodated by side chains of A-R6, A-W9, B-Y93 and provided the Cap's orientation suitable for forming H-bond between hydroxyphenyl of B-Y93 and NH of carbamate. The isopropyl function was directed at B-R6 and A-Y93. The End Cap occupying the binding site I and corresponding imidazole interacted with a flexible region of chain A, particularly with A-A30, A-G33, A-L34. Furthermore, the model predicted that Val-carbamate moiety was oriented towards D-I of chain B, thereby providing H-bonds with NH of B-Y161 and a side chain of B-E92. Based on the analysis of AV-4025 binding mode, we have suggested that well-tuned

substitutions introduced in the linker may occupy either the pocket in D-I formed by side chains of B-T95 and B-R56 or space between A-L31 and A-D10 and consequently increase interaction surface area. Another opportunity to enhance the binding affinity is to fill the room in the cap-binding site II more tightly by replacing isopropyl with a more bulky function. Additionally, as mentioned above, R30A substitution results in loss of H-bonding with carbamate moiety. Thus, another chance to improve activity is to realize more tight contact with a flexible linker by modifying the isopropyl group for a more large fragment.

Following our molecular modeling efforts, we have designed a series of AV-4025 structural analogs – a small-sized virtual library contained synthetically accessible compounds. Phenyl fragment of the spacer was substituted with aryl functions, cycloalkyl, and alkyl moieties, readily available in our proprietary collection, at positions R¹ or/and R² (see Table 1). In addition, we also replaced a canonical isopropyl moiety at the Cap region by S- and R-phenyl fragment. All the proposed structures were then docked using the developed model and ranked by virtual scoring values as well as synthesized and evaluated in a replicon-based assay against six different HCV genotypes in the absence of human plasma.

Modeling suggested that the linker substitutions of 1.1–1.4 are surrounded by residues B-T95, B-R56, A-L31, and A-D10 (Fig. 6). Cation- π interactions with the guanidinium function of B-R56 were predicted for phenyl, naphthyl, biphenyl of 1.1, 1.2, and 1.4, respectively. The orientation of 4-*tert*-butylphenyl introduced in the linker of 1.3 was not suitable for providing cation- π interaction, but it more tightly

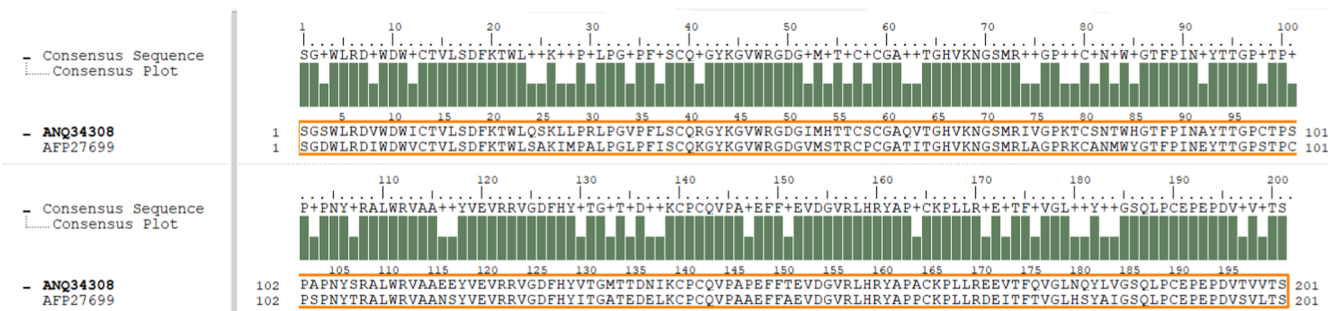


Fig. 3. The alignment of amino-acid sequences for N-terminal α -helix, linker region and D-I for NS5A gT1b (ANQ34308) and gT3a (AFP27699).

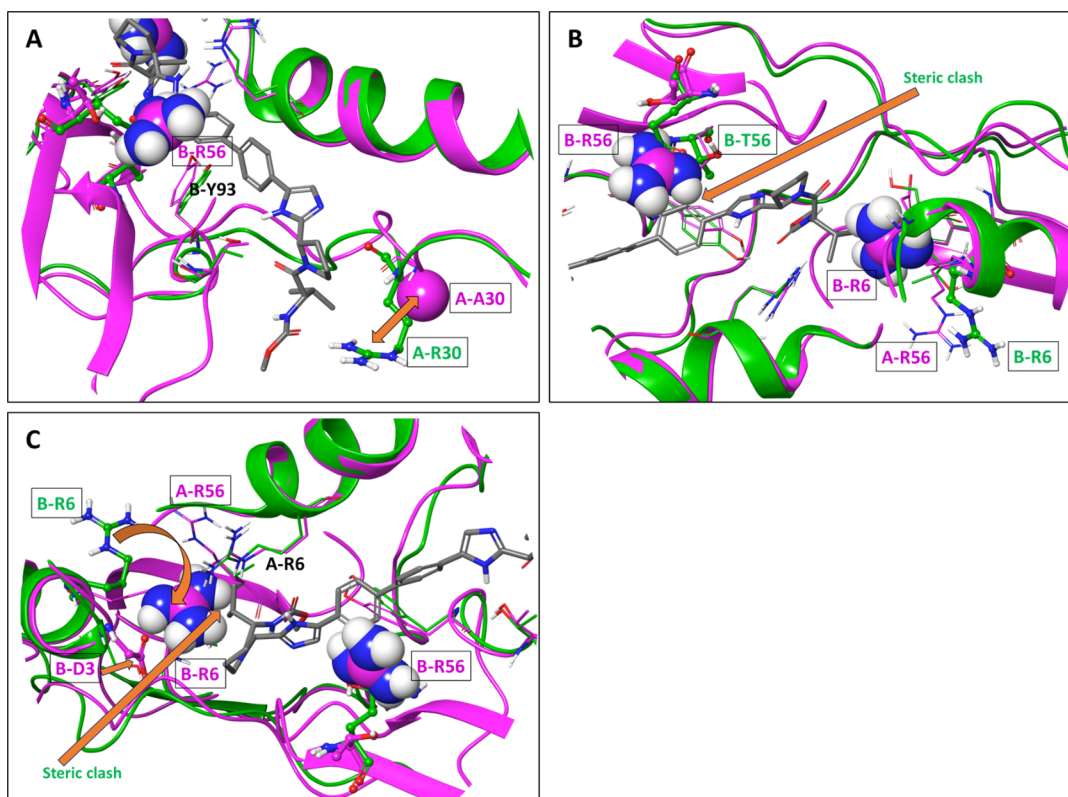


Fig. 4. The superposition of two structural models for the *N*-terminal region of NS5A: gt1b (green) in complex with daclatasvir and gt3a (magenta) described in the present article. Daclatasvir is represented by grey color and a thick tube model. (A) Cap binding site I: A-R30 is represented by a thick tube model, the side chain of A-A30 is represented by a space-filling model. (B) The cleft occupied by a linker of an inhibitor: B-T56 and the side chain of B-R56 are represented by a thick tube and a space-filling model, respectively. The orange arrow indicates the possible steric collision between the biphenyl linker of daclatasvir and the guanidinium function of B-R56. (C) Cap binding site II: A-R6 and B-D3 are represented by a thick tube model, the guanidinium group of B-R6 is depicted as a space-filling model. The orange curved arrow indicates the predicted replacement of the B-R6 side chain observing in the model of gt3a. The orange arrow indicates the possible steric clash between the B-R6 side chain and End Cap of daclatasvir.

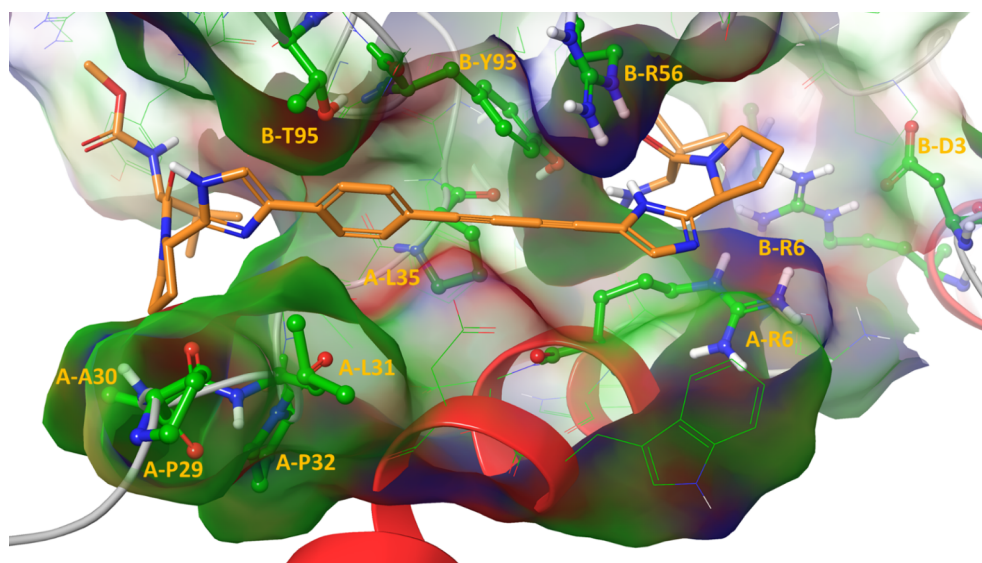


Fig. 5. The predicted binding mode of AV-4025 (orange) to NS5A gT3a. Key residues are represented by a ball-and-stick model, while the inhibitor is depicted as a tube model.

occupied the space between side chains of A-L31 and A-D10. Methyl and fluorine at the R² position of **1.5** and **1.6** demonstrated contacts with B-Y93 and pyrrolidine of A-P35, meanwhile phenyl introduced in the spacer was placed in a similar manner as for **1.1**.

According to the results presented in Table 1, the introduction of the

unsubstituted phenyl ring (compound **1.1**) led to two-fold increase in activity against gT3a in contrast to the parent compound. The substitution with 4-*tert*-butylphenyl (**1.3**) resulted in the same potency towards gT3a (EC₅₀ = 1286 pM), however the activity against gT1a significantly dropped. Compound **1.2** containing 2-naphthyl substituent

Table 1
Emodel scoring function value and antiviral activity of novel NS5A HCV inhibitors 1.1–1.24.

ID	Common structure	Emodel NS5A g3a	IC ₅₀ , pM					
			gT1b	gT1a	gT2a	gT3a	gT4a	gT5a
AV-4025		-66.43	5.1 ± 2.8	215 ± 39	84 ± 27	2449 ± 444	28 ± 6	407 ± 90
1.1		-88.89	2.1 ± 1.6	72 ± 9	30 ± 7	1311 ± 812	7.1 ± 1.3	129 ± 78
1.2		-84.92	1.6 ± 0.5	248 ± 13	28 ± 8	864 ± 307	8.4 ± 1	267 ± 68
1.3		-98.15	1.7 ± 0.7	642 ± 279	1684 ± 553	1286 ± 446	11 ± 1.8	356 ± 50
1.4		-84.22	1.2 ± 0.5	470 ± 71	449 ± 190	2785 ± 601	19.2 ± 2.1	763 ± 77

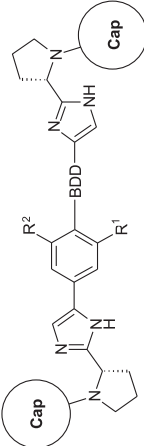
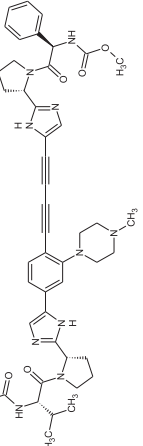
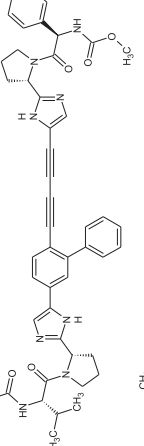
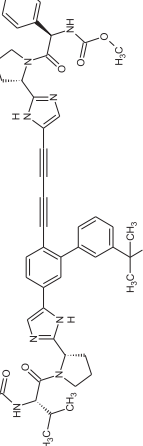
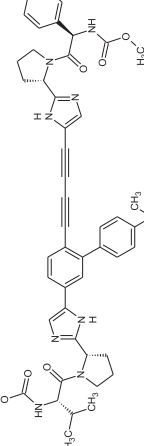
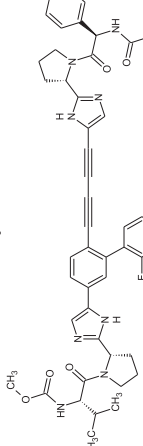
(continued on next page)

Table 1 (continued)

ID	Common structure	Emodel NS5A gt3a	IC ₅₀ , pM		gT2a	gT3a	gT4a	gT5a
			gT1b	gT1a				
1.5		-99.53	2.2 ± 1	37 ± 7	7.9 ± 2.3	364 ± 35	5.9 ± 0.2	27 ± 2
1.6		-91.57	1.5 ± 0.6	64 ± 15	15.2 ± 5.8	459 ± 57	19.2 ± 10.5	120 ± 3
1.7		-105.5	6.8 ± 1.6	276 ± 35	16 ± 4.2	329 ± 94	36 ± 12	126 ± 30
1.8		-65.48	12 ± 1	758 ± 98	431 ± 175	10700 ± 1934	423 ± 120	6400 ± 1501
1.9		-93.88	6.1 ± 3.3	210 ± 89	7 ± 3.1	629 ± 316	11.6 ± 6.6	100 ± 10
1.10		-65.42	12 ± 4.2	1340 ± 231	120 ± 42	4917 ± 1538	123 ± 101	200

(continued on next page)

Table 1 (continued)

ID	Common structure	E _{model} NS5A gt3a	IC ₅₀ , pM					
			gT1b	gT1a	gT2a	gT3a	gT4a	gT5a
1.11		-100.9	34 ± 16	473 ± 159	143 ± 56	> 10000	> 10000	3100
1.12		-103.31	2.9 ± 6	45 ± 12	3.3 ± 0.9	34 ± 11	7.6 ± 1.5	26 ± 3
1.13		-115.9	1.2 ± 0.4	2296 ± 1538	4.6 ± 1.9	362 ± 87	10.3 ± 1	693 ± 69
1.14		-101.02	1.2 ± 0.2	1069 ± 199	104 ± 38	93 ± 4	7.3 ± 0.3	107 ± 9
1.15		-104.48	3.3 ± 1.5	28 ± 9.4	1.0 ± 0.5	16 ± 8.4	5.7 ± 2.1	19 ± 6.34
1.16		-108.69	1.5 ± 0.4	138 ± 33	12.8 ± 9.9	38 ± 9	10.8 ± 1.8	52 ± 6

(continued on next page)

Table 1 (continued)

ID	Common structure	Emodel NS5A gt3a	IC ₅₀ , pM					
			gT1b	gT1a	gT2a	gT3a	gT4a	gT5a
1.17		-95.1	4.2 ± 2.1	113 ± 65.2	23 ± 4	353 ± 100.32	548 ± 205	1400 ± 393
1.18		-122.34	1.8 ± 0.4	626 ± 94	33 ± 12	123 ± 20	11 ± 3.8	122 ± 44
1.19		-108.28	1.6 ± 0.8	418 ± 124	4.6 ± 1.2	64 ± 9	6.3 ± 1.9	131 ± 24
1.20		NA	1.9 ± 0.7	124 ± 18	3 ± 2	26 ± 4	9.6 ± 1.5	19 ± 3

(continued on next page)

Table 1 (continued)

ID	Common structure	Emodel NS5A gt3a	IC ₅₀ , pM					
			gT1b	gT1a	gT2a	gT3a	gT4a	gT5a
1.21		NA	1.4 ± 0.5	51 ± 12	5 ± 1.4	20 ± 2	11.8 ± 3.9	26 ± 4
1.22		-99.8	1.5 ± 0.4	214 ± 46	12.6 ± 4.7	40 ± 7	7.7 ± 2.5	19 ± 3
1.23		-108.8	1.7 ± 0.8	257 ± 21	14.2 ± 3.1	91 ± 10	9.2 ± 2	35 ± 9
1.24		-111.66	1.8 ± 0.7	72 ± 12	10.6 ± 1.8	35 ± 3	11 ± 2.2	27 ± 1

NA – not applicable.

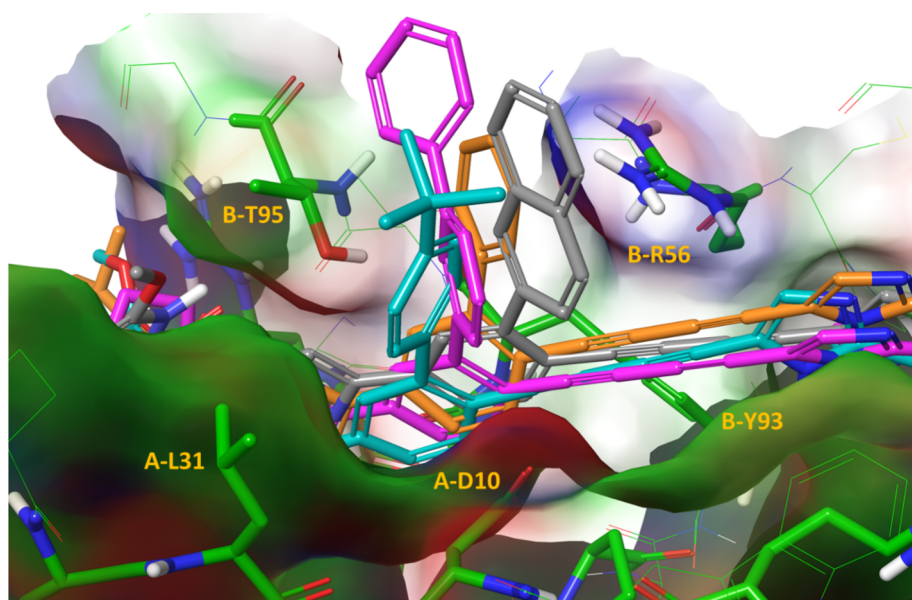


Fig. 6. The predicted binding modes of 1.1 (orange), 1.2 (grey), 1.3 (cyan) and 1.4 (magenta) to NS5A gT3a. Inhibitors and key binding residues are depicted as a thick tube model.

demonstrated picomolar activity against gT3a ($EC_{50} = 864$ pM). A decrease in the potency of 1.4 can be explained by the torsional angle between phenyl rings in biphenyl-3-yl moiety, and their relative spatial orientations resulted in unfavorable steric clashes with protein structure, while 2-naphthyl is coplanar with the unsubstituted phenyl. For compounds 1.5 and 1.6 containing methyl and fluorine substituents at position R^2 , respectively, we have obtained higher scorings in contrast to 1.1. These molecules were predicted to form more contacts along with a protein interface, specifically with the pyrrolidine ring of A-P35 and the side chain of B-Y93. Indeed, both molecules demonstrated an improved activity against all the HCV isoforms evaluated vs. compound 1.1.

In our previous SAR study we demonstrated that stereo-configuration of Caps dramatically affects antiviral activity towards gT1b.¹⁸ *De facto*, AV-4025 contains four (*S*)-chiral centers, and it showed the highest antiviral efficiency among combinatorial partners. Herein, we investigated the impact of the replacement of *N*-Moc-valine group with *N*-Moc-phenylglycine in both Caps and exploited molecular docking to assess the differences in putative binding modes (Fig. 7A). *N*-Moc-(*R*)-phenylglycine moiety of 1.7 occupied the binding site I, phenyl fragment of the Cap provided contacts with B-Y161 and B-R160 side chains. Methyl group of carbamate was predicted to interact with A-L34 and A-G33 of the flexible region, as well as NH of the same Cap formed H-bond with B-E92 of D-I. The (*S*)-phenylglycine of 1.8 interacted with A-G33 and A-A30, while carbamate was placed near B-Y161 and B-R160 interacting with their side chains, however, without H-bond B-E92. The pyrrolidine ring attached to this Cap was oriented to contact with B-T95. Other binding mode was predicted for compound 1.9 during docking studies (Fig. 7B). Cap-associated phenyl ring was positioned deeply within site II thereby occupying the pocket formed by B-I37, B-F36, and A-Y93 and providing hydrophobic interactions with them. Carbamate of this Cap interacted with A-F36 and A-D3 side chains by methyl function. Noteworthy, NH formed H-bond with hydroxyphenyl of B-Y93. Hydrogen bonding between A-R6 and amide of pyrrolidine moiety was observed as well. In contrast, (*S*)-phenyl group of 1.10 was directed towards B-Y93 as well as interacted with the side chains of both R6, A-D3, and B-Y93. Carbamate function was predicted to provide contacts with B-R6, A-Y93, B-P35, B-F36, and B-G60. Finally, compounds 1.7 and 1.9 exhibited dramatically lower docking scores rather than 1.8 and 1.10 (Table 1). This fact can be explained by the presence of H-bonds and more appropriate orientations of phenyl

fragments in the Cap-binding sites I and II for 1.7 and 1.9, respectively, oppositely to their stereoisomers.

Biological testing showed that the replacement of *N*-Moc-*L*-valine with *N*-Moc-(*S*)-phenylglycine in 1.8 and 1.10 leads to a 2-fold reduction in the target activity towards gT1b as well as against other genotypes (Table 1). Then, we have demonstrated that the opposite stereo-configuration at this chiral point improves gT3a activity, and this

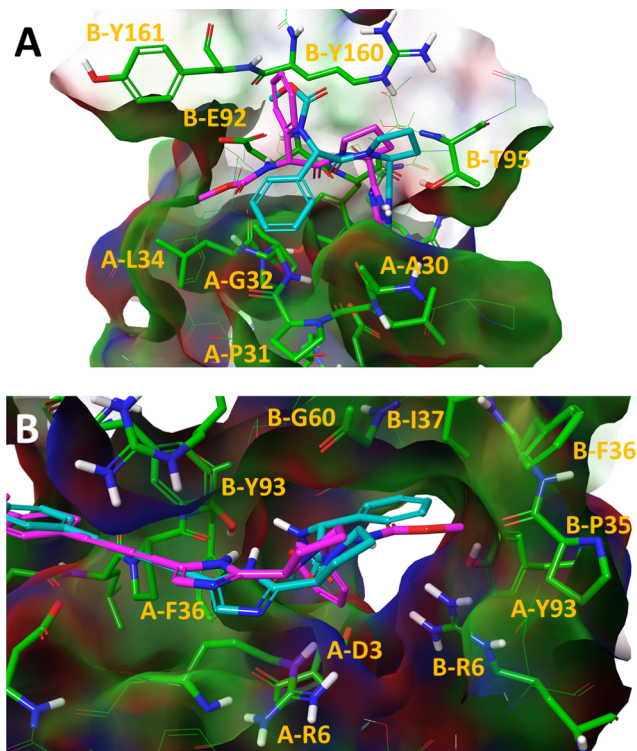


Fig. 7. (A) Putative binding modes of 1.7 (magenta) and 1.8 (cyan) with phenylglycine instead of *L*-Val in the Cap proximal to phenyl fragment of a linker. (B) Putative binding modes of 1.9 (cyan) and 1.10 (magenta) with phenylglycine instead of *L*-Val in the Cap distal to phenyl fragment of a linker. Compounds and key binding residues are represented as a thick tube model.

correlates with the results of our docking simulations. Indeed, **1.7** and **1.9** showed EC_{50} values of 329 and 629 pM, respectively. This observation is consistent with the data reported earlier by the group from Bristol-Myers Squibb.³¹ Interestingly, modification of the Cap that is distal to the phenyl fragment in the linker has more impact on the antiviral profile as compared to the proximal one. These results are in agreement with our data published previously.¹⁸ Compound with (*R*)-chiral point at the proximal Cap was 23-fold less active than AV-4025, while *R*-configuration at the distal Cap resulted in a 120-fold reduction in the desired activity. These SAR observations indicate that Caps bind within different sites. Moreover, during the modeling, we have found that the distal Cap interacts with Y93, a key amino acid residue associated with resistance.

Taking into account the results of molecular docking and SAR studies, compound **1.9** was selected as the most promising starting point for subsequent morphing. As exemplified in Fig. 8, compounds were predicted to provide benefit H-bond with B-Y93 as well as tightly occupied the interface formed by *N*-terminal α -helix, protein linker region and D-I. Surprisingly, the modeling was not resulted in the highly scored binding modes for compounds **1.20** and **1.21** with substitutions in both R^1 and R^2 positions. The values of Emodel scoring function for other compounds are lower than -95 . Inhibitors **1.12**–**1.24** exhibited firm picomolar activity against gT3a, excepting methylpiperazine analog **1.11** demonstrated EC_{50} value > 10 nM despite quite high docking score (Emodel = -100.9). It likely indicates that aryl substitutions introduced at the linker part are more preferable than saturated cycles. However, this observation cannot be explained in the scope of the present model and requires further computational efforts. Replacing the distal Cap with *N*-Moc-(*R*)-phenylglycine and the addition of phenyl ring at position R^1 resulted in compound **1.12** with an EC_{50} value of 34 pM. The addition of *tert*-butyl group at phenyl fragment reduced activity (**1.13** and **1.14**). However, compound **1.16** bearing dimethylamino phenyl moiety inhibited HCV replication with a similar to **1.12** manner, except gT1a and gT2a isoforms. Introducing 2,3-difluorophenyl fragment (compound **1.15**) led to enhanced activity, particularly against gT3a isoform ($EC_{50} = 16$ pM, two-fold more active than **1.12**). Compounds **1.17**–**1.19** bearing more bulky functionalities as well as more flexible ones (**1.22**–**1.24**) did not demonstrate significant improvements. Considering the results obtained for compounds **1.5** and **1.6**, we investigated the impact of methyl- or fluoro-substituent at position R^2 of compound **1.12** on gT3a replication. These modifications resulted in compounds **1.20** and **1.21**, respectively, with

slightly improved potency as compared to **1.12**. Summarizing, compounds **1.12** and **1.15** demonstrated an enhanced virologic profile in contrast to AV-4025 and inhibited the replication of six HCV genotypes with an activity in low picomolar range.

2.2. Chemistry

The key step for the preparation of compounds **1.1**–**1.24** was Sonogashira cross-coupling reaction between 2-[(2*S*)-1-acylpyrrolidin-2-yl]-5-(4-buta-1,3-diyn-1-ylphenyl)-1*H*-imidazole and 2-[(2*S*)-1-acetylpyrrolidin-2-yl]-5-iodo-1*H*-imidazole or between 2-[(2*S*)-1-acetylpyrrolidin-2-yl]-5-(4-iodophenyl)-1*H*-imidazole and 2-[(2*S*)-1-acetylpyrrolidin-2-yl]-4-buta-1,3-diyn-1-yl-1*H*-imidazole with a subsequent modification of pyrrolidine fragment to get the final Cap-containing molecules with the desired stereo-configuration. Building blocks (BBs) were radially synthesized as described previously¹⁸ or obtained from commercial sources. The target compounds were synthesized starting from the reaction between BB (II) and *tert*-butyl (2*S*)-2-(4-iodo-1*H*-imidazol-2-yl)pyrrolidine-1-carboxylate (III) after the elimination of trimethylsilyl group from BB (I) (Scheme 1). Products (IV) were obtained in good yield and used for further versatile transformation. Thus, intermediate (IV) was deprotected ($-Boc$) upon alkaline conditions resulted in compound (V). Acylation of (V) with Moc-*L*-Valine, *N*-Moc-(*R*)-phenylglycine or *N*-Moc-(*S*)-phenylglycine led to the desired product **1.1**–**1.24** ($\cdot 2HCl$) in moderate-to-high yields (see exp. section). The final products were obtained as the optically pure stereoisomers containing four chiral centers. The structure of substituents R^1 and R^2 as well as Caps attached to (V) via acylation can readily be identified in Table 1.

3. Biological evaluation

3.1. Cell-based assay

Antiviral activity of the synthesized compounds was evaluated against six distinct genotypes of NS5A HCV (gT1b, gT1a, gT2a, gT3a, gT4a, and gT5a). The standard human hepatoma cell line Huh7 harboring the HCV replicon was used as a test system. The obtained results are summarized in Table 1. As shown in Table 1, inhibitors **1.7** and **1.9** containing phenyl in the End Caps at *R*-configuration are 13- and 6.8-times more active with respect to gT3a than AV-4025, respectively. At the same time, compounds **1.8** and **1.10** bearing phenyl in the end caps

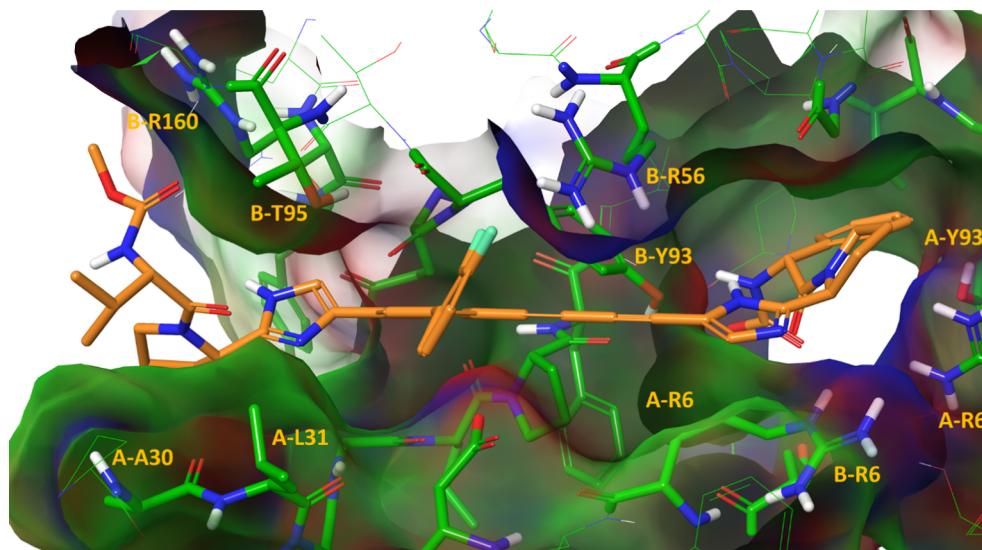
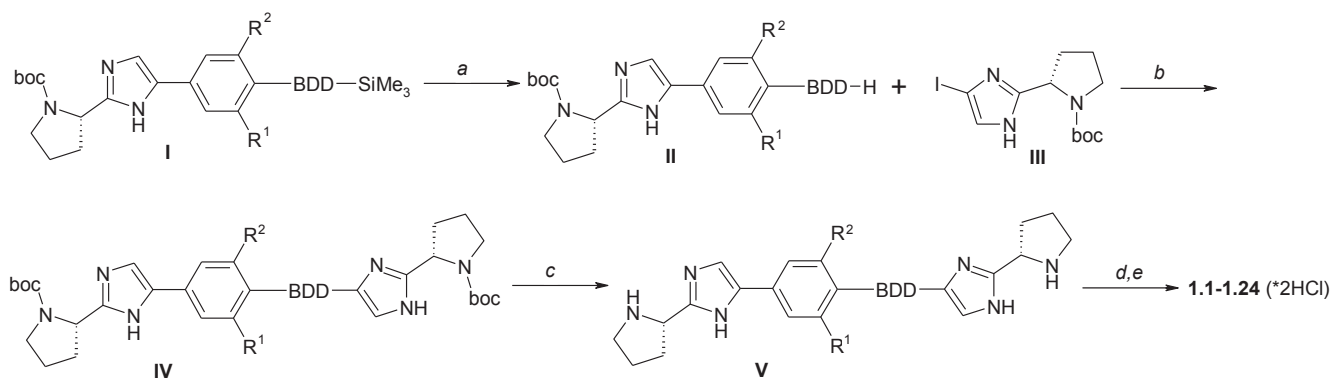


Fig. 8. Predicted binding mode for compound **1.15** (orange) to NS5A gT3a that illustrates the impact of Cap and linker modifications on ligand-protein interactions. Compound and key residues are represented as a thick tube model.



Scheme 1. The common route for the preparation of compounds **1.1–1.24** (·2HCl): BDD – buta-1,3-diyne-1,4-diyl, R^1 and R^2 are listed in Table 1 below. Reagents and conditions: (a) K_2CO_3 , THF, MeOH; (b) $Pd(PPh_3)_4$, CuI, THF (or DMF), Et_3N , 40–45 °C; (c) HCl, dioxane; (d) for Moc-L-Val-OH: HATU, DMF, DIPEA, 4 °C, while for Moc-(R)-PhGly-OH or Moc-(S)-PhGly-OH: HATU, MeCN, DIPEA, –20 °C; (e) HCl, dioxane (or in EtOAc).

at S-configuration are 2.6- and 1.1-times less active against gT3a than the parent molecule. These data correlate well with the results obtained during the molecular docking study (Fig. 9). In general, inhibitors containing bulky substituents simultaneously in the linker (R^1) and in the Cap fragment are significantly more active with respect to NS5A HCV in contrast to AV-4025. For instance, salt compositions of compounds **1.12**, **1.15**, **1.16**, **1.20**, **1.21** and **1.23** inhibit gT1b isoform with EC_{50} value in the range of 1.5–2.9 pM, gT1a with EC_{50} = 28.0–260.0 pM, gT2a with EC_{50} = 1.0–14.0 pM, gT3a with EC_{50} = 16.0–91.0 pM, gT4a with EC_{50} = 5.7–12.0 pM, and gT5a with EC_{50} = 19.0–52.0 pM. In this series of compounds, the most attractive are compounds **1.12** and **1.15**, which are the most active against gT3a (EC_{50} = 34.0 pM and EC_{50} = 16.0 pM, respectively). The weakest activity was shown for compound **1.11**·4HCl containing 4-methyl piperazine substituent.

3.2. Pharmacokinetics in rats

Pharmacokinetic profile (PK) for compounds **1.12**·2HCl, **1.15** and **1.15**·2HCl was determined in rats (for details see exp. section below). The obtained data is summarized in Table 2. As shown in Table 2, compound **1.12**·2HCl significantly exceeds its analogs in its PK properties and can be reasonably regarded as the most attractive candidate for further clinical evaluation. For instance, upon PO administration, **1.12**·2HCl demonstrated 43-times more favorable AUC value in contrast to **1.15**·2HCl and 13-times higher bioavailability.

4. Conclusion

Recently, we have described the synthesis and extensive biological evaluation of small-molecule HCV NS5A inhibitor AV-4025.¹⁸ In the present paper, in order to improve antiviral activity, we have performed a rational design of novel pan-genotypic HCV NS5A inhibitors (AV-4025 analogs) containing modified linker and Caps. Docking study with AV-4025 has provided a valuable insight into the potential binding mode of the parent compound and allowed us to firmly indicate key diversity points for enhancing antiviral efficiency. Especially, the substitution of phenyl moiety in the spacer by relatively bulky aromatic fragments was considered as the most promising strategy to achieve the greater activity. Furthermore, we predicted that the substitution of isopropyl moiety in the Cap regions by phenyl fragment with inverse stereo-configuration might also lead to reliable improvements. Based on the obtained results, we designed a small-sized virtual library of structures bearing appropriate substituents attached to the predicted diversity points and carried out molecular docking study. Taking into account the obtained scoring values and synthetic capabilities, we have synthesized 24 compounds using combinatorial schemes to evaluate

their antiviral activity and estimate the prediction power of the developed *in silico* model. The biological evaluation confirmed the high predictive ability of the model, and we observed consistency between scoring values and activities (Fig. 9). The biological testing has revealed compound **1.12** as the most promising lead candidate. The compound effectively inhibited HCV replication in human hepatoma cell line Huh7, demonstrated pan-specific picomolar activity against six HCV isoforms, and did not show any cytotoxicity. In particular, it blocked the replication of HCV gT3a with an EC_{50} value of 34 pM, whereas the parent compound (AV-4025) was 126-times less active. PK study performed for lead compound **1.12** has provided impressive results making this molecule very attractive for subsequent clinical evaluation.

5. Experimental section

5.1. Chemistry

Starting materials, as a rule, are commercially available products. All chemicals and solvents were used as received from suppliers without further purification. The crude reaction mixtures were concentrated under reduced pressure by removing organic solvents. Several starting compounds and BBs were synthesized in according to the reported synthetic procedures: *tert*-butyl (2*S*)-2-(4-iodo-1*H*-imidazol-2-yl)-pyrrolidine-1-carboxylate,³² (2*S*)-2-(5-{4-[4-(trimethylsilyl)buta-1,3-diyne-1-yl]phenyl}-1*H*-imidazol-2-yl)pyrrolidine-1-carboxylate,¹⁸ methyl [(1*S*)-1-{[(2*S*)-2-(4-iodo-1*H*-imidazol-2-yl)pyrrolidin-1-yl]carbonyl}-2-

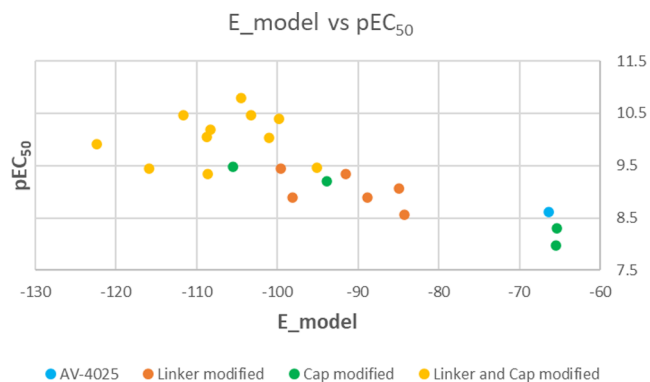


Fig. 9. The plot represents the relationship between docking score values (E_{model}) and potency against HCV gT3a (pEC_{50}). Parent compound AV-4025 is highlighted in cyan, compounds **1.1–1.6** are highlighted in orange, compounds **1.7–1.10** are highlighted in green, compounds **1.12–1.24** are highlighted in yellow. Compound **1.11** was excluded from the plot due to its exact EC_{50} value is unknown, **1.20** and **1.21** were excluded due to the absence of adequate binding modes.

Table 2
PK profile for compounds **1.12**·2HCl, **1.15** and **1.15**·2HCl.

Compound ID	1.12·2HCl		1.15		1.15·2HCl	
	IV, 2 mg/kg	PO, 10 mg/kg	IV, 2 mg/kg	PO, 10 mg/kg	IV, 2 mg/kg	PO, 10 mg/kg
AUC _{INF} , h ² ng/ml	8327	13,098	285	61.7	2734	328.7
AUC _{last} , h ² ng/ml	8256	12,591	279	58.7	2724	270.8
C _{max} , ng/ml	7763	2980	114	38.3	1155	15.2
T _{max} , h	0.083	2.0	0.083	1.0	0.083	0.7
T _{1/2} , h	1.2	1.6	4.6	0.6	3.2	2.5
MRT _{INF,obs} , h	1.3	3.1	4.7	1.5	3.3	0.4
MRT _{last} , h	1.2	2.8	4.2	1.4	3.2	0.3
F _{abs} , %	–	31.0	–	4.3	–	2.4

methylpropyl]carbamate,³³ (S)-3-methyl-1-oxo-1-((S)-2-(5-((4-(2-((S)-pyrrolidin-2-yl)-1H-imidazol-5-yl)phenyl)buta-1,3-diynyl)-1H-imidazol-2-yl)pyrrolidin-1-yl)butan-2-ylcarbamate trihydrochloride,¹⁸ 2-((2S)-1-(1-*tert*-butoxyethenyl)pyrrolidin-2-yl)-5-ethynyl-1H-imidazole.³⁴ Nuclear magnetic resonance (NMR) spectra were recorded using Bruker DPX-400 spectrometer at room temperature (rt) with tetramethyl silane as an internal standard. The chemical shifts (δ) are reported in parts per million (ppm), and the signals are reported as s (singlet), d (doublet), t (triplet), q (quartet), m (multiplet), or br s (broad singlet). The purities of the final compounds were determined by HPLC and were > 98%. The HPLC conditions for assessing purity were as follows: Shimadzu HPLC, XBridge C18, 4.6 mm \times 250 mm (3.5 μ m); gradient of 0.1% TFA in 5% acetonitrile/water (A) and 0.1% TFA acetonitrile (B); flow rate, 0.5 ml/min; acquisition time, 20 min; detection wavelengths, UV 214 and 254 nm. The preparative HPLC system included two sets of Shimadzu LC-8A pumps, a Shimadzu SCL 10Avp controller, and a Shimadzu SPD 10Avp detector. A Reprosil-Pur C18-AQ 10 μ m, 250 mm \times 20 mm column was used. The mobile phase was a gradient of 0.1% TFA in water (A) and 0.1% TFA in acetonitrile (B). LC/MS analysis was carried out using PE Sciex API 165 system equipped with electrospray in positive ion mode, [M + H]⁺, and Shimadzu HPLC system equipped with a Waters XBridge C18 3.5 μ m column (4.6 mm \times 150 mm). High-resolution mass spectrometry (HRMS) data was obtained using Bruker microTOF II instrument with electrospray ionization (ESI) in the Department of Structural Studies of Zelinsky Institute of Organic Chemistry, Moscow. The measurements were performed in positive ion mode (interface capillary voltage – 4500 V) or in negative ion mode (3200 V). The analyzed mass range was from *m/z* 50 to *m/z* 3000 Da, and external or internal calibration was performed with Electrospray Calibrant Solution (Fluka). Syringe injection was used for solutions in acetonitrile, methanol, or water (flow rate 3 ml/min). Nitrogen was used as the dry gas; the interface temperature was set at 180 °C.

5.1.1. General procedure for compounds 1.1–1.24

To a solution of *tert*-butyl (2S)-2-(5-((4-(trimethylsilyl)buta-1,3-diyn-1-yl)phenyl)-1H-imidazol-2-yl)pyrrolidine-1-carboxylate (**I**, 0.75–2 mmol) in THF (5 ml) and methanol (5 ml) K₂CO₃ (2.25–3.39 mmol) was added and the resulting mixture was stirred under argon atmosphere for 2 h, then filtered and rotovapped. To a solution of the obtained *tert*-butyl (2S)-2-[5-(4-buta-1,3-diyn-1-yl-phenyl)-1H-imidazol-2-yl]pyrrolidine-1-carboxylate (**II**) in THF (6 ml) or DMF (4 ml) *tert*-butyl (S)-2-(5-iodo-1H-imidazol-2-yl)-pyrrolidine-1-carboxylate (**III**) (0.5–0.85 mmol), TEA (2 ml), Pd(PPh₃)₄ (0.025–0.043 mmol), and CuI (0.05–0.085 mmol) were added. The resulting mixture was then stirred under argon at 40–45 °C for 15–48 h. Then, the mixture was diluted with DCM, filtered, washed with saturated NH₄Cl solution, rotovapped and subjected to HPLC to give *tert*-butyl (2S)-2-[5-((4-(2-((2S)-1-(*tert*-butoxycarbonyl)pyrrolidin-2-yl)-1H-imidazol-5-yl)buta-1,3-diyn-1-yl)phenyl)-1H-imidazol-2-yl]pyrrolidine-1-carboxylate **IV** in 28–35% yield. To a solution of **IV** (0.24 mmol)

in 3.5 ml of dioxane 4 M HCl solution in dioxane (3.5 ml) was added. The mixture was stirred for 15 h, then rotovapped to obtain 2-((2S)-pyrrolidin-2-yl)-5-[4-(4-(2-((2S)-pyrrolidin-2-yl)-1H-imidazol-5-yl)buta-1,3-diyn-1-yl)phenyl]-1H-imidazole (**V**). Intermediate (**V**) was then dissolved in DMF (5 ml) or MeCN (5 ml) and Caps were added as follows: *N*-Moc-*L*-valine (0.51–0.61 mmol), HATU (0.24–0.72 mmol) and DIPEA (2.3–2.4 mmol) or *N*-Moc-*R*-(or *S*-)phenylglycine (0.21 mmol or 0.34 mmol) and HATU (0.34 mmol) and DIPEA (1 mmol or 1.7 mmol, after cooling to –20 °C). The resulting mixture was stirred in a fridge for 2–4 h, then was diluted with DCM, washed with 5% citric acid solution (for phenylglycine derivative with 5% Na₂CO₃ solution), dried over Na₂SO₄, rotovapped and subjected to HPLC to give the desired products **1.1–1.4** with 61–65% yield, **1.5** (35%), **1.6** (31%), **1.7** and **1.8** (82%), **1.9** and **1.10** (56%), **1.11** (69%), **1.12–1.24** (28–77%). The corresponding dihydrochlorides or tetrahydrochloride (for compound **1.17**) were obtained by the addition of 4 M HCl (*an excess*) solution in dioxane (or in EtOAc) to the final compound dissolved in acetone (~4 ml). The resulting mixture was diluted with 4 ml of ether, the precipitate was filtered, washed with ether and dried *in vacuo* to afford the desired salts.

Methyl [(S)-1-((S)-2-{5-[(4-(2-((S)-1-((S)-2-methoxycarbonylamino-3-methylbutyl)pyrrolidin-2-yl)-1H-imidazol-5-yl)bi-phenyl-2-yl)buta-1,3-diynyl]-1H-imidazol-2-yl}pyrrolidine-1-carbonyl)-2-methylpropyl]-carbamate dihydrochloride (1.1·2HCl): LC/MS 787 (M + H)⁺. ¹H NMR (DMSO-*d*₆, 400 MHz) δ 15.41 (brs, 0.4H), 14.90 (brs, 0.7H), 8.30 (s, 0.1H), 8.28 (s, 0.9H), 8.04 (s, 1H), 7.98 (d, *J* = 8.0 Hz, 1H), 7.93 (brs, 2H), 7.89 (d, *J* = 8.0 Hz, 1H), 7.66 (m, 2H), 7.51 (m, 3H), 7.27 (m, 1.77H), 7.18 (m, 0.12H), 6.85 (m, 0.11H), 5.74 (m, 0.05H), 5.45 (m, 0.05H), 5.18 (d, *J* = 6.8 Hz, 0.95H) 5.03 (dd, *J*₁ = 8.0 Hz, *J*₂ = 6.0 Hz, 0.95H), 4.12 (t, *J* = 7.6 Hz, 1H), 4.06 (t, *J* = 8.0 Hz, 1H), 3.98 (m, 1H), 3.81 (m, 3H), 3.53 (2 s, 5.45H), 3.40 (s, 0.35H), 3.29 (s, 0.2H), 2.37 (m, 1H), 2.26 (m, 1H), 2.18 (m, 2H), 2.10 (m, 2H), 2.00 (m, 4H), 0.78 (m, 12H). ESIHRMS *m/z* calcd for C₄₄H₅₀N₈O₆ [M + H]⁺ 787.3926; found 787.3908.

Methyl [(S)-1-((S)-2-{5-[(4-(2-((S)-1-((S)-2-methoxycarbonylamino-3-methylbutyl)pyrrolidin-2-yl)-1H-imidazol-5-yl)-2-[naphthalen-2-yl]phenyl)buta-1,3-diynyl]-1H-imidazol-2-yl}pyrrolidine-1-carbonyl)-2-methylpropyl]-carbamate dihydrochloride (1.2·2HCl): LC/MS molecular ion peak was at 837 (M + H)⁺, ¹H NMR (DMSO-*d*₆, 400 MHz) δ 15.46 (brs, 0.4H), 14.90 (brs, 0.7H), 8.32 (s, 0.1H), 8.30 (s, 0.9H), 8.20 (m, 2H), 8.07 (d, *J* = 8.8 Hz, 1H), 8.02 (m, 3H), 7.94 (m, 1H), 7.88 (brs, 2H), 7.82 (m, 1H), 7.60 (m, 2H), 7.27 (m, 1.8H), 7.15 (m, 0.1H), 6.84 (m, 0.1H), 5.75 (m, 0.05H), 5.42 (m, 0.05H), 5.18 (d, *J* = 6.8 Hz, 0.95H), 5.01 (dd, *J*₁ = 7.6 Hz, *J*₂ = 5.6 Hz, 0.95H), 4.12 (t, *J* = 7.6 Hz, 1H), 4.05 (t, *J* = 8.0 Hz, 1H), 3.99 (m, 1H), 3.80 (m, 3H), 3.53, 3.54 (2 s, 5.5H), 3.35 (s, 0.3H), 3.30 (s, 0.2H), 2.38 (m, 1H), 2.21 (m, 3H), 2.09 (m, 2H), 1.97 (m, 4H), 0.80 (m, 12H). ESIHRMS *m/z* calcd for C₄₈H₅₂N₈O₆ [M + H]⁺ 837.4082; found 837.4069.

*Methyl [(S)-1-((S)-2-{5-[(4-(3'-*tert*-butyl-5-{2-[(S)-1-((S)-2-methoxycarbonylamino-3-methyl-butyl)-pyrrolidin-2-yl]-3H-imidazol-4-yl)-bi-phenyl-2-yl)-buta-1,3-diynyl]-1H-imidazol-2-yl}pyrrolidine-1-carbonyl)-*

2-methyl-propyl]-carbamate dihydrochloride (1.3:2HCl): LC/MS 844 (M+H)⁺. ¹H NMR (DMSO-*d*₆, 400 MHz) δ 15.39 (brs, 0.5H), 14.84 (brs, 0.6H), 8.29 (s, 0.1H), 8.26 (s, 0.9H), 8.05 (s, 1H), 7.94 (m, 1H), 7.88 (m, 1H), 7.83 (brs, 0.85H), 7.74 (s, 1H), 7.48 (m, 3H), 7.28 (m, 1.7H), 7.13 (m, 0.03H), 6.86 (m, 0.05H), 5.73 (m, 0.03H), 5.39 (m, 0.04H), 5.17 (t, *J* = 6.8 Hz, 0.97H), 5.02 (dd, *J*₁ = 7.6 Hz, *J*₂ = 5.2 Hz, 0.96H), 4.12 (t, *J* = 7.6 Hz, 1H), 4.05 (t, *J* = 8.0 Hz, 1H), 3.98 (m, 1H), 3.81 (m, 3H), 3.53 (2 s, 5.5H), 3.40 (s, 0.3H), 3.30 (s, 0.2H), 2.37 (m, 1H), 2.06–2.27 (m, 5H), 1.98 (m, 4H), 1.35 (s, 9H), 0.75–0.93 (m, 12H). ESIHRMS *m/z* calcd for C₄₈H₅₈N₈O₆ [M+H]⁺ 843.4552; found 843.4541.

Methyl {(S)-1-[(S)-2-(5-[4-(5-(2-[(S)-1-[(S)-2-methoxycarbonylamino-3-methyl-butyl]-pyrrolidin-2-yl)-3H-imidazol-4-yl]-[1,1';3',1'']terphenyl-2-yl)-buta-1,3-dienyl]-1H-imidazol-2-yl)-pyrrolidine-1-carbonyl]-2-methyl-propyl]-carbamate dihydrochloride (1.4:2HCl): LC/MS 864 (M+H)⁺. ¹H NMR (DMSO-*d*₆, 400 MHz) δ 15.49 (brs, 0.65H), 14.91 (brs, 0.85H), 8.32 (s, 0.1H), 8.30 (s, 0.9H), 8.19 (s, 1H), 8.00, 8.02 (2 s, 1H), 7.92 (m, 2.8H), 7.81 (m, 2H), 7.77 (m, 1H), 7.70 (m, 1H), 7.63 (m, 1H), 7.49 (m, 2H), 7.39 (m, 1H), 7.27 (m, 1.75H), 7.17 (m, 0.13H), 6.86 (m, 0.12H), 5.76 (m, 0.05H), 5.44 (m, 0.08H), 5.18 (t, *J* = 7.0 Hz, 0.95H), 5.03 (dd, *J*₁ = 7.6 Hz, *J*₂ = 5.6 Hz, 0.92H), 4.11 (t, *J* = 7.8 Hz, 1H), 4.05 (t, *J* = 8.0 Hz, 1H), 4.00 (m, 1H), 3.81 (m, 3H), 3.53 (s, 5.5H), 3.37 (s, 0.3H), 3.29 (s, 0.2H), 2.37 (m, 1H), 1.92–2.29 (m, 9H), 0.74–0.93 (m, 12H). ESIHRMS *m/z* calcd for C₅₀H₅₄N₈O₆ [M+H]⁺ 863.4239; found 863.4238.

Methyl {(S)-1-[(S)-2-(5-[5-(2-[(S)-1-[(S)-2-(methoxycarbonylamino)-3-methylbutyl]pyrrolidin-2-yl)-1H-imidazol-5-yl]-3-methylbiphenyl-2-yl]buta-1,3-dienyl)-1H-imidazol-2-yl]pyrrolidine-1-carbonyl]-2-methylpropyl]-carbamate (1.5:2HCl): LC/MS 801 (M+H)⁺. ¹H NMR (DMSO-*d*₆, 400 MHz) δ 15.12 (brs, 0.6H), 14.72 (brs, 0.7H), 8.22 (s, 1H), 7.90 (s, 1H), 7.79 (m, 2H), 7.61 (m, 2H), 7.53 (m, 2H), 7.47 (m, 1H), 7.27 (d, *J* = 8.4 Hz, 1.8H), 7.07 (m, 0.1H), 6.86 (m, 0.1H), 5.66 (m, 0.05H), 5.32 (m, 0.08H), 5.15 (t, *J* = 6.8 Hz, 0.95H), 5.01 (dd, *J*₁ = 7.6 Hz, *J*₂ = 4.8 Hz, 0.92H), 4.11 (t, *J* = 7.8 Hz, 1H), 4.04 (t, *J* = 8.0 Hz, 1H), 3.93 (m, 1H), 3.83 (m, 1H), 3.77 (m, 2H), 3.53, 3.54 (2 s, 5.5H), 3.41 (s, 0.3H), 3.30 (s, 0.2H), 2.54 (s, 3H), 2.37 (m, 1H), 1.91–2.24 (m, 9H), 0.76–0.92 (m, 12H). ESIHRMS *m/z* calcd for C₄₅H₅₂N₈O₆ [M+H]⁺ 801.44082; found 801.4090.

Methyl {(S)-1-[(S)-2-(5-[3-fluoro-5-(2-[(S)-1-[(S)-2-(methoxycarbonylamino)-3-methylbutyl]pyrrolidin-2-yl)-1H-imidazol-5-yl]biphenyl-2-yl]buta-1,3-dienyl)-1H-imidazol-2-yl]pyrrolidine-1-carbonyl]-2-methylpropyl]-carbamate dihydrochloride (1.6:2HCl): LC/MS 805 (M+H)⁺. ¹H NMR (DMSO-*d*₆, 400 MHz) δ 14.86 (brs, 0.6H), 8.34 (s, 0.1H), 8.32 (s, 0.9H), 8.04 (m, 1H), 7.92 (s, 2H), 7.68 (m, 2H), 7.53 (m, 3H), 7.26 (t, *J* = 8.0 Hz, 1.77H), 7.15 (m, 0.15H), 6.85 (m, 0.08H), 5.69 (m, 0.05H), 5.40 (m, 0.08H), 5.16 (t, *J* = 6.8 Hz, 0.95H), 5.02 (dd, *J*₁ = 7.6 Hz, *J*₂ = 5.2 Hz, 0.92H), 4.11 (t, *J* = 7.6 Hz, 1H), 4.05 (t, *J* = 8.0 Hz, 1H), 3.97 (m, 1H), 3.80 (m, 3H), 3.53, 3.54 (2 s, 5.5H), 3.40 (s, 0.3H), 3.31 (s, 0.2H), 2.36 (m, 1H), 2.05–2.30 (m, 5H), 1.98 (m, 4H), 1.35 (s, 9H), 0.75–0.92 (m, 12H). ESIHRMS *m/z* calcd for C₄₄H₄₉N₈O₆ [M+H]⁺ 805.3832; found 805.3828.

Methyl {(R)-1-[(S)-2-(5-[4-(2-[(S)-1-[(S)-2-(methoxycarbonylamino)-3-methylbutanoyl]pyrrolidin-2-yl)-1H-imidazol-5-yl]phenyl]buta-1,3-dienyl)-1H-imidazol-2-yl]pyrrolidine-1-yl]-2-oxo-1-phenylethyl]-carbamate dihydrochloride (1.7:2HCl): LC/MS 745 (M+H)⁺. ¹H NMR (DMSO-*d*₆, 400 MHz) δ 15.30 (brs, 0.3H), 14.69 (brs, 0.8H), 8.23 (s, 0.9H), 8.00 (d, *J* = 8.4 Hz, 1.8H), 7.93 (s, 1H), 7.78 (m, 2.1H), 7.71 (d, *J* = 7.6 Hz, 1H), 7.33 (m, 5.5H), 7.16 (m, 0.17H), 7.07 (m, 0.23H), 6.99 (m, 0.3H), 5.83 (d, *J* = 8.0 Hz, 0.1H), 5.58 (m, 0.05H), 5.51 (d, *J* = 8.0 Hz, 0.8H), 5.43 (m, 0.15H), 5.39 (d, *J* = 7.2 Hz, 0.1H), 5.25 (m, 0.9H), 5.05 (m, 0.9H), 4.12 (t, *J* = 7.6 Hz, 1H), 3.97 (m, 1H), 3.82 (m, 2H), 3.51, 3.52 (2 s, 5.7H), 3.43 (s, 0.3H), 3.15 (m, 1H), 2.26 (m, 2H), 2.15 (m, 1H), 2.02 (m, 5H), 1.88 (m, 1H), 0.88 (t, *J* = 7.2 Hz, 0.7H), 0.79, 0.82 (2d, *J* = 6.8 Hz, 5.3H). ESIHRMS *m/z* calcd for C₄₁H₄₄N₈O₆ [M+H]⁺ 745.3456; found 745.3457.

Methyl {(S)-1-[(S)-2-(5-[4-(2-[(S)-1-[(S)-2-(methoxycarbonylamino)-3-methylbutanoyl]pyrrolidin-2-yl)-1H-imidazol-5-yl]phenyl]buta-1,3-dienyl)-1H-imidazol-2-yl]pyrrolidine-1-yl]-2-oxo-1-phenylethyl]-carbamate dihydrochloride (1.8:2HCl): LC/MS 745 (M+H)⁺. ¹H NMR (DMSO-*d*₆,

400 MHz) δ 15.17 (brs, 0.4H), 14.71 (brs, 0.7H), 8.26 (s, 0.1H), 8.17 (s, 0.9H), 7.99 (m, 0.35H), 7.93 (m, 3.6H), 7.78 (m, 2H), 7.71 (m, 0.05H), 7.43 (m, 0.25H), 7.38 (m, 0.5H), 7.30 (m, 5.3H), 7.16 (m, 0.05H), 5.57 (d, *J* = 8.8 Hz, 0.9H), 5.43 (m, 0.1H), 5.32 (m, 0.1H), 5.22 (m, 0.9H), 5.05 (m, 1H), 4.07 (t, *J* = 7.6 Hz, 1H), 3.78 (m, 4H), 3.54, 3.55 (2 s, 5.4H), 3.44 (s, 0.3H), 3.39 (s, 0.3H), 2.36 (m, 1H), 2.26 (m, 1H), 2.06 (m, 7H), 0.88 (t, *J* = 6.8 Hz, 0.6H), 0.79, 0.82 (2d, *J* = 6.8 Hz, 5.4H). ESIHRMS *m/z* calcd for C₄₁H₄₄N₈O₆ [M+H]⁺ 745.3456; found 745.3445.

Methyl {(R)-1-[(S)-2-(5-[4-(2-[(S)-1-[(S)-2-(methoxycarbonylamino)-2-phenylacetyl]pyrrolidin-2-yl)-1H-imidazol-5-yl]phenyl]buta-1,3-dienyl)-1H-imidazol-2-yl]pyrrolidine-1-yl]-3-methyl-1-oxobutan-2-yl]-carbamate dihydrochloride (1.9:2HCl): LC/MS 745 (M+H)⁺. ¹H NMR (DMSO-*d*₆, 400 MHz) δ 15.34 (brs, 0.6H), 14.82 (brs, 0.8H), 8.20 (s, 1H), 7.96 (m, 3H), 7.85 (d, *J* = 8.0 Hz, 0.7H), 7.77 (m, 2H), 7.66 (m, 0.3H), 7.31 (m, 6H), 5.74 (m, 0.1H), 5.51 (m, 0.8H), 5.17 (t, *J* = 6.8 Hz, 0.9H), 5.09 (m, 0.8H), 5.00 (d, *J* = 7.6 Hz, 0.2H), 4.91 (m, 0.2H), 4.12 (t, *J* = 7.6 Hz, 1H), 3.98 (m, 1H), 3.83 (m, 1H), 3.70 (m, 1H), 3.54, 3.55 (2 s, 5.5H), 3.46 (s, 0.3H), 3.41 (m, 1H), 3.31 (s, 0.2H), 2.37 (m, 1H), 2.20 (m, 3H), 2.02 (m, 5H), 0.91 (m, 0.4H), 0.76, 0.82 (2d, *J* = 6.4 Hz, 5.6H). ESIHRMS *m/z* calcd for C₄₁H₄₄N₈O₆ [M+H]⁺ 745.3456; found 745.3443.

Methyl {(S)-1-[(S)-2-(5-[4-(2-[(S)-1-[(S)-2-(methoxycarbonylamino)-2-phenylacetyl]pyrrolidin-2-yl)-1H-imidazol-5-yl]phenyl]buta-1,3-dienyl)-1H-imidazol-2-yl]pyrrolidine-1-yl]-3-methyl-1-oxobutan-2-yl]-carbamate dihydrochloride (1.10:2HCl): LC/MS 745 (M+H)⁺. ¹H NMR (DMSO-*d*₆, 400 MHz) δ 15.35 (brs, 0.5H), 14.80 (brs, 0.6H), 8.20 (s, 1H), 7.98 (m, 3H), 7.78 (m, 2.2H), 7.68 (m, 0.7H), 7.60 (s, 0.1H), 7.32 (m, 5.3H), 7.16 (m, 0.5H), 6.96 (m, 0.2H), 5.73 (m, 0.05H), 5.56 (m, 0.15H), 5.49 (m, 0.8H), 5.32 (m, 0.15H), 5.17 (m, 1.05H), 5.09 (m, 0.8H), 4.12 (t, *J* = 7.6 Hz, 1H), 3.97 (m, 1H), 3.86 (m, 2H), 3.53, 3.54 (2 s, 5.9H), 3.31 (s, 0.1H), 3.11 (m, 1H), 2.37 (m, 1H), 2.06 (m, 7H), 1.84 (m, 1H), 0.91 (m, 0.3H), 0.76, 0.82 (2d, *J* = 6.8 Hz, 5.7H). ESIHRMS *m/z* calcd for C₄₁H₄₄N₈O₆ [M+H]⁺ 745.3456; found 745.3448.

Methyl {(S)-1-[(S)-2-(5-[4-(2-[(S)-1-[(R)-2-(methoxycarbonylamino)-2-phenylacetyl]pyrrolidin-2-yl)-1H-imidazol-5-yl]buta-1,3-dienyl]-3-(4-methylpiperazin-1-yl)phenyl)-1H-imidazol-2-yl]pyrrolidine-1-carbonyl]-2-methylpropyl]-carbamate tetrahydrochloride (1.11:4HCl): LC/MS: 822 (M+H)⁺. ¹H NMR (DMSO-*d*₆, 400 MHz) δ 15.64 (brs, 0.6H), 14.90 (brs, 0.8H), 11.25 (brs, 1H), 8.29 (s, 0.05H), 8.26 (s, 0.95H), 7.99 (s, 0.8H), 7.86 (m, 0.2H), 7.69 (m, 2.8H), 7.58 (m, 1.2H), 7.34 (m, 4.6H), 7.26 (d, *J* = 8.0 Hz, 0.8H), 7.16 (m, 0.4H), 6.97 (m, 0.2H), 5.76 (m, 0.04H), 5.55 (m, 0.13H), 5.49 (d, *J* = 8.0 Hz, 0.77H), 5.30 (d, *J* = 8.0 Hz, 0.12H) 5.19 (t, *J* = 7.2 Hz, 1H), 5.10 (m, 0.94H), 4.12 (t, *J* = 7.6 Hz, 1H), 4.02 (m, 1H), 3.89 (m, 1H), 3.80 (m, 3H), 3.54 (m, 2H), 3.53, 3.54 (2 s, 5.8H), 3.36 (m, 2.2H), 3.23 (m, 2H), 3.10 (m, 1H), 2.85 (d, *J* = 4.0 Hz, 3H), 2.37 (m, 1H), 1.91–2.24 (m, 6H), 1.84 (m, 1H), 0.93 (d, *J* = 6.8 Hz, 0.2H), 0.90 (d, *J* = 6.8 Hz, 0.2H), 0.83 (d, *J* = 6.8 Hz, 2.8H), 0.76 (d, *J* = 6.8 Hz, 2.8H). ESIHRMS *m/z* calcd for C₄₆H₅₄N₁₀O₆ [M+H]⁺ 843.4300; found 745.3457.

Methyl {(S)-1-[(S)-2-(5-[6-(2-[(S)-1-[(R)-2-(methoxycarbonylamino)-2-phenylacetyl]pyrrolidin-2-yl)-1H-imidazol-5-yl]buta-1,3-dienyl]biphenyl-3-yl)-1H-imidazol-2-yl]pyrrolidine-1-carbonyl]-2-methylpropyl]-carbamate dihydrochloride (1.12:2HCl, 66%): LC/MS 821 (M+H)⁺. ¹H NMR (DMSO-*d*₆, 400 MHz) δ 15.35 (brs, 0.6H), 14.84 (brs, 0.6H), 8.30 (s, 0.1H), 8.28 (s, 0.9H), 8.02 (m, 1H), 7.96 (m, 1.8H), 7.90 (m, 1H), 7.82 (m, 0.2H), 7.67 (m, 2.8H), 7.55 (m, 2H), 7.49 (m, 1H), 7.26–7.37 (m, 5.5H), 7.13 (m, 0.45H), 6.95 (m, 0.25H), 5.71 (m, 0.05H), 5.55 (m, 0.15H), 5.47 (d, *J* = 7.6 Hz, 0.8H), 5.30 (d, *J* = 7.6 Hz, 0.15H), 5.17 (t, *J* = 6.8 Hz, 1H), 5.07 (m, 0.85H), 4.12 (t, *J* = 7.6 Hz, 1H), 3.96 (m, 1H), 3.85 (m, 2H), 3.53, 3.54 (2 s, 5.9H), 3.30 (s, 0.1H), 3.11 (m, 1H), 1.90–2.21 (m, 5H), 1.83 (m, 1H), 0.92 (d, *J* = 6.8 Hz, 0.15H), 0.89 (d, *J* = 6.8 Hz, 0.15H), 0.83 (d, *J* = 6.8 Hz, 2.85H), 0.76 (d, *J* = 6.8 Hz, 2.85H). ESIHRMS *m/z* calcd for C₄₇H₄₈N₈O₆ [M+H]⁺ 821.3769; found 821.3761.

Methyl {(S)-1-[(S)-2-(5-[4'-tert-butyl-6-[(2-[(S)-1-[(R)-2-(methoxycarbonylamino)-2-phenylacetyl]pyrrolidin-2-yl)-1H-imidazol-5-yl]buta-1,3-dienyl]biphenyl-3-yl)-1H-imidazol-2-yl]pyrrolidine-1-carbonyl]-2-methylpropyl]-carbamate dihydrochloride (1.13:2HCl, 75%): LC/MS 877 (M+H)⁺. ¹H NMR (DMSO-*d*₆, 400 MHz) δ 15.34 (brs, 0.5H), 14.86 (brs,

0.6H), 8.30 (s, 0.1H), 8.28 (s, 0.9H), 8.02 (s, 1H), 7.96 (m, 1.7H), 7.89 (m, 1H), 7.82 (d, $J = 8.0$ Hz, 0.2H), 7.67 (d, $J = 8.0$ Hz, 0.8H), 7.62 (d, $J = 8.4$ Hz, 2H), 7.56 (d, $J = 8.4$ Hz, 2H), 7.36 (m, 4H), 7.29 (m, 1H), 7.12 (m, 0.4H), 6.95 (m, 0.2H), 5.73 (m, 0.04H), 5.55 (m, 0.12H), 5.47 (d, $J = 7.6$ Hz, 0.8H), 5.30 (d, $J = 7.6$ Hz, 0.14H) 5.17 (t, $J = 6.8$ Hz, 1H), 5.08 (m, 0.9H), 4.12 (t, $J = 7.6$ Hz, 1H), 3.97 (m, 1H), 3.85 (m, 2H), 3.52, 3.54 (2 s, 5.8H), 3.29 (s, 0.2H), 3.10 (m, 1H), 2.37 (m, 1H), 1.90–2.21 (m, 6H), 1.83 (m, 1H), 1.35 (s, 9H), 0.92 (d, $J = 6.8$ Hz, 0.2H), 0.89 (d, $J = 6.8$ Hz, 0.2H), 0.83 (d, $J = 6.8$ Hz, 2.8H), 0.76 (d, $J = 6.8$ Hz, 2.8H). ESIHRMS m/z calcd for $C_{51}H_{56}N_8O_6$ $[M+H]^+$ 877.4395; found 877.4377.

Methyl $\{(S)-1-[(S)-2-(5-(3'-tert-butyl-6-[(2-((S)-1-[(R)-2-(methoxycarbonylamino)-2-phenylacetyl]pyrrolidin-2-yl)-1H-imidazol-5-yl)]buta-1,3-dienyl]biphenyl-3-yl)-1H-imidazol-2-yl]pyrrolidine-1-carbonyl]-2-methylpropyl\}-carbamate dihydrochloride$ (1.14·2HCl, 56%): LC/MS 877 ($M+H$)⁺. ¹H NMR (DMSO-*d*₆, 400 MHz) δ 15.42 (brs, 0.4H), 14.84 (brs, 0.6H), 8.30 (s, 0.1H), 8.27 (s, 0.9H), 8.07 (m, 1H), 7.95 (m, 1H), 7.89 (m, 1.7H), 7.82 (d, $J = 7.6$ Hz, 0.2H), 7.73 (s, 1H), 7.66 (d, $J = 7.6$ Hz, 0.8H), 7.48 (m, 3.2H), 7.35 (m, 4.4H), 7.29 (m, 1H), 7.27 (d, $J = 8.8$ Hz, 0.8H), 7.12 (m, 0.5H), 6.93 (m, 0.25H), 5.74 (m, 0.05H), 5.54 (m, 0.14H), 5.47 (d, $J = 7.6$ Hz, 0.77H), 5.30 (d, $J = 7.6$ Hz, 0.18H) 5.18 (t, $J = 6.8$ Hz, 1H), 5.07 (m, 0.9H), 4.12 (t, $J = 7.6$ Hz, 1H), 3.98 (m, 1H), 3.85 (m, 2H), 3.52, 3.54 (2 s, 5.8H), 3.30 (s, 0.2H), 3.10 (m, 1H), 2.38 (m, 1H), 2.18 (m, 2H), 2.00 (m, 1H), 1.97 (m, 3H), 1.83 (m, 1H), 1.36, 1.37 (2 s, 9H), 0.92 (d, $J = 6.8$ Hz, 0.2H), 0.89 (d, $J = 6.8$ Hz, 0.2H), 0.83 (d, $J = 6.8$ Hz, 2.8H), 0.76 (d, $J = 6.8$ Hz, 2.8H). ESIHRMS m/z calcd for $C_{51}H_{56}N_8O_6$ $[M+H]^+$ 877.4395; found 877.4372.

Methyl $\{(S)-1-[(S)-2-(5-(2',3'-difluoro-6-[(2-((S)-1-[(R)-2-(methoxycarbonylamino)-2-phenylacetyl]pyrrolidin-2-yl)-1H-imidazol-5-yl)]buta-1,3-dienyl]biphenyl-3-yl)-1H-imidazol-2-yl]pyrrolidine-1-carbonyl]-2-methylpropyl\}-carbamate dihydrochloride$ (1.15·2HCl, 63%): LC/MS 857 ($M+H$)⁺. ¹H NMR (DMSO-*d*₆, 400 MHz) δ 15.31 (brs, 0.4H), 14.81 (brs, 0.7H), 8.26 (s, 0.95H), 8.07 (m, 1.95H), 7.93 (m, 1.74H), 7.81 (m, 0.25H), 7.61 (m, 1.92H), 7.35 (m, 7.28H), 7.11 (m, 0.58H), 6.93 (m, 0.33H), 5.70 (m, 0.08H), 5.52 (m, 0.13H), 5.47 (d, $J = 8.0$ Hz, 0.76H), 5.29 (m, 0.16H), 5.16 (t, $J = 7.0$ Hz, 1H), 5.06 (m, 0.87H), 4.11 (t, $J = 8.0$ Hz, 1H), 3.96 (m, 1H), 3.84 (m, 2H), 3.53, 3.54 (2 s, 5.76H), 3.30 (s, 0.24H), 3.10 (m, 1H), 2.37 (m, 1H), 2.04 (m, 7H), 1.82 (m, 1H), 0.89, 0.91 (2d, $J = 6.8$ Hz, 0.55H), 0.76, 0.82 (2d, $J = 6.8$ Hz, 5.45H). ESIHRMS m/z calcd for $C_{47}H_{46}FN_8O_6$ $[M+H]^+$ 857.3581; found 857.3584.

Methyl $\{(S)-1-[(S)-2-(5-(4'-(dimethylamino)-6-[(2-((S)-1-[(R)-2-(methoxycarbonylamino)-2-phenylacetyl]pyrrolidin-2-yl)-1H-imidazol-5-yl)]buta-1,3-dienyl]biphenyl-3-yl)-1H-imidazol-2-yl]pyrrolidine-1-carbonyl]-2-methylpropyl\}-carbamate trihydrochloride$ (1.16·2HCl, 74%): LC/MS 864 ($M+H$)⁺. ¹H NMR (DMSO-*d*₆, 400 MHz) δ 15.50 (brs, 0.6H), 14.93 (brs, 0.9H), 8.30 (s, 0.1H), 8.27 (s, 0.9H), 8.07 (s, 0.8H), 8.04 (s, 1H), 7.91 (m, 1H), 7.86 (m, 1H), 7.77 (m, 0.2H), 7.67 (m, 2.8H), 7.35 (m, 4.7H), 7.26 (d, $J = 8.4$ Hz, 1H), 7.14 (m, 2H), 6.99 (m, 0.3H), 5.77 (m, 0.1H), 5.64 (m, 0.15H), 5.48 (d, $J = 7.6$ Hz, 0.75H), 5.32 (d, $J = 7.6$ Hz, 0.15H) 5.19 (t, $J = 6.8$ Hz, 0.95H), 5.12 (m, 0.9H), 4.12 (t, $J = 7.6$ Hz, 1H), 4.00 (m, 1H), 3.85 (m, 2H), 3.52, 3.54 (2 s, 5.8H), 3.30 (s, 0.2H), 3.10 (m, 1H), 3.04 (s, 6H), 2.37 (m, 1H), 1.92–2.23 (m, 6H), 1.84 (m, 1H), 0.92 (d, $J = 6.8$ Hz, 0.2H), 0.90 (d, $J = 6.8$ Hz, 0.2H), 0.83 (d, $J = 6.8$ Hz, 2.8H), 0.76 (d, $J = 6.8$ Hz, 2.8H). ESIHRMS m/z calcd for $C_{49}H_{53}N_9O_6$ $[M+H]^+$ 864.4191; found 864.4192.

Methyl $\{(S)-1-[(S)-2-(5-(6-[(2-((S)-1-[(R)-2-(methoxycarbonylamino)-2-phenylacetyl]pyrrolidin-2-yl)-1H-imidazol-5-yl)]buta-1,3-dienyl]-4'-(4-methylpiperazin-1-yl)biphenyl-3-yl)-1H-imidazol-2-yl]pyrrolidine-1-carbonyl]-2-methylpropyl\}-carbamate tetrahydrochloride$ (1.17·4HCl, 57%): LC/MS 919 ($M+H$)⁺. ¹H NMR (DMSO-*d*₆, 400 MHz) δ 15.52 (brs, 0.6H), 14.91 (brs, 0.7H), 11.19 (brs, 1H), 8.29 (s, 0.1H), 8.26 (s, 0.9H), 8.04 (m, 1.1H), 7.98 (s, 0.8H), 7.87 (m, 2.3H), 7.68 (d, $J = 8.0$ Hz, 0.75H), 7.62 (m, 2.2H), 7.34 (m, 4.7H), 7.26 (d, $J = 8.4$ Hz, 1H), 7.14 (m, 2.5H), 6.96 (m, 0.25H), 5.76

(m, 0.02H), 5.57 (m, 0.07H), 5.48 (d, $J = 7.6$ Hz, 0.8H), 5.30 (d, $J = 7.6$ Hz, 0.11H) 5.19 (t, $J = 7.2$ Hz, 1H), 5.09 (m, 1H), 4.12 (t, $J = 7.6$ Hz, 1H), 3.99 (m, 3H), 3.85 (m, 2H), 3.53, 3.54 (2 s, 5.8H), 3.50 (m, 2H), 3.30 (s, 0.2H), 3.17 (m, 5H), 2.82 (d, $J = 4.4$ Hz, 3H), 2.36 (m, 1H), 2.14 (m, 3H), 1.97 (m, 3H), 1.83 (m, 1H), 0.92 (d, $J = 6.8$ Hz, 0.2H), 0.89 (d, $J = 6.8$ Hz, 0.2H), 0.83 (d, $J = 6.8$ Hz, 2.8H), 0.76 (d, $J = 6.8$ Hz, 2.8H). ESIHRMS m/z calcd for $C_{52}H_{58}N_{10}O_6$ $[M+H]^+$ 919.4613; found 919.4603.

Methyl $\{(S)-1-[(S)-2-(5-(6-[(2-((S)-1-[(R)-2-(methoxycarbonylamino)-2-phenylacetyl]pyrrolidin-2-yl)-1H-imidazol-5-yl)]buta-1,3-dienyl]-1',1':3',1''-terphenyl-3-yl)-1H-imidazol-2-yl]pyrrolidine-1-carbonyl]-2-methylpropyl\}-carbamate dihydrochloride$ (1.18·2HCl, 62%): LC/MS 897 ($M+H$)⁺. ¹H NMR (DMSO-*d*₆, 400 MHz) δ 15.42 (brs, 0.6H), 14.86 (brs, 0.8H), 8.32 (s, 0.1H), 8.30 (s, 0.9H), 8.17 (m, 1H), 7.99 (m, 1H), 7.94 (m, 2.9H), 7.80 (m, 3.4H), 7.67 (m, 3H), 7.50 (m, 2.3H), 7.37 (m, 5.6H), 7.26 (d, $J = 8.4$ Hz, 1H), 7.08 (m, 0.5H), 6.93 (m, 0.3H), 5.74 (m, 0.06H), 5.54 (m, 0.15H), 5.47 (d, $J = 7.6$ Hz, 0.77H), 5.29 (d, $J = 7.6$ Hz, 0.16H) 5.18 (t, $J = 7.2$ Hz, 0.97H), 5.07 (m, 0.89H), 4.12 (t, $J = 7.6$ Hz, 1H), 3.99 (m, 1H), 3.84 (m, 2H), 3.51, 3.53 (2 s, 5.8H), 3.30 (s, 0.2H), 3.10 (m, 1H), 2.38 (m, 1H), 1.90–2.22 (m, 6H), 1.83 (m, 1H), 0.92 (d, $J = 6.8$ Hz, 0.2H), 0.89 (d, $J = 6.8$ Hz, 0.2H), 0.81 (d, $J = 6.8$ Hz, 2.8H), 0.75 (d, $J = 6.8$ Hz, 2.8H). ESIHRMS m/z calcd for $C_{53}H_{52}N_8O_6$ $[M+H]^+$ 897.4082; found 897.4083.

Methyl $\{(S)-1-[(S)-2-(5-(6-[(2-((S)-1-[(R)-2-(methoxycarbonylamino)-2-phenylacetyl]pyrrolidin-2-yl)-1H-imidazol-5-yl)]buta-1,3-dienyl]-1',1':4',1''-terphenyl-3-yl)-1H-imidazol-2-yl]pyrrolidine-1-carbonyl]-2-methylpropyl\}-carbamate dihydrochloride$ (1.19·2HCl, 62%): LC/MS 897 ($M+H$)⁺. ¹H NMR (DMSO-*d*₆, 400 MHz) δ 15.38 (brs, 0.5H), 14.85 (brs, 0.6H), 8.29 (s, 1H), 8.09 (m, 1H), 7.99 (m, 1H), 7.92 (m, 1.6H), 7.86 (m, 1.9H), 7.79 (m, 3.7H), 7.65 (m, 0.7H), 7.51 (m, 2H), 7.35 (m, 5.5H), 7.08 (m, 0.38H), 6.92 (m, 0.22H), 5.73 (m, 0.06H), 5.52 (m, 0.15H), 5.46 (d, $J = 8.0$ Hz, 0.8H), 5.28 (d, $J = 8.0$ Hz, 0.2H) 5.18 (t, $J = 6.8$ Hz, 0.94H), 5.06 (m, 0.85H), 4.12 (t, $J = 7.6$ Hz, 1H), 3.98 (m, 1H), 3.84 (m, 2H), 3.53, 3.54 (2 s, 3H), 3.49 (s, 2.75H), 3.31 (s, 0.25H), 3.09 (m, 1H), 2.38 (m, 1H), 2.18 (m, 2H), 2.09 (m, 1H), 2.03 (m, 1H), 1.93 (m, 2H), 1.81 (m, 1H), 0.92 (d, $J = 6.8$ Hz, 0.2H), 0.90 (d, $J = 6.8$ Hz, 0.2H), 0.83 (d, $J = 6.8$ Hz, 2.8H), 0.77 (d, $J = 6.8$ Hz, 2.8H). ESIHRMS m/z calcd for $C_{53}H_{52}N_8O_6$ $[M+H]^+$ 897.4082; found 897.4065.

Methyl $\{(S)-1-[(S)-2-(5-(6-[(2-((S)-1-[(R)-2-(methoxycarbonylamino)-2-phenylacetyl]pyrrolidin-2-yl)-1H-imidazol-5-yl)]buta-1,3-dienyl]-5-methylbiphenyl-3-yl)-1H-imidazol-2-yl]pyrrolidine-1-carbonyl]-2-methylpropyl\}-carbamate dihydrochloride$ (1.20·2HCl, 77%): LC/MS 835 ($M+H$)⁺. ¹H NMR (DMSO-*d*₆, 400 MHz) δ 15.21 (brs, 0.6H), 14.78 (brs, 0.7H), 8.25 (s, 0.1H), 8.23 (s, 0.9H), 7.93 (m, 1.8H), 7.82 (m, 1.1H), 7.63 (m, 2.8H), 7.53 (m, 2.2H), 7.48 (m, 1H), 7.35 (m, 4.5H), 7.26 (d, $J = 8.4$ Hz, 0.9H), 7.12 (m, 0.5H), 6.94 (m, 0.2H), 5.69 (m, 0.05H), 5.54 (m, 0.1H), 5.47 (d, $J = 7.6$ Hz, 0.8H), 5.29 (d, $J = 7.6$ Hz, 0.15H), 5.16 (t, $J = 7.0$ Hz, 1H), 5.07 (m, 0.9H), 4.11 (t, $J = 7.6$ Hz, 1H), 3.95 (m, 1H), 3.84 (m, 2H), 3.53, 3.54 (2 s, 5.8H), 3.30 (s, 0.2H), 3.10 (m, 1H), 2.55 (s, 3H), 2.37 (m, 1H), 1.89–2.22 (m, 6H), 1.83 (m, 1H), 0.91 (d, $J = 6.8$ Hz, 0.2H), 0.89 (d, $J = 6.8$ Hz, 0.2H), 0.82 (d, $J = 6.8$ Hz, 2.8H), 0.76 (d, $J = 6.8$ Hz, 2.8H). ESIHRMS m/z calcd for $C_{48}H_{50}N_8O_6$ $[M+H]^+$ 835.3926; found 835.3905.

Methyl $\{(1R)-2-[(2S)-2-(5-[4-(3-fluoro-5-{2-[(2S)-1-[(2S)-2-[(methoxycarbonylamino]-3-methylbutanoyl]pyrrolidin-2-yl)-1H-imidazol-5-yl]biphenyl-2-yl]buta-1,3-dien-1-yl]-1H-imidazol-2-yl]pyrrolidin-1-yl]-2-oxo-1-phenylethyl]carbamate$ (1.21·2HCl, 71%): LC/MS 839 ($M+H$)⁺. ¹H NMR (DMSO-*d*₆, 400 MHz) δ 14.86 (brs, 0.6H), 8.35 (s, 0.1H), 8.32 (s, 0.9H), 8.05 (m, 1H), 7.97 (s, 0.8H), 7.93 (s, 1H), 7.68 (m, 2.8H), 7.55 (m, 3.2H), 7.35 (m, 4.5H), 7.25 (d, $J = 8.8$ Hz, 0.9H), 7.12 (m, 0.5H), 6.95 (m, 0.2H), 5.69 (m, 0.05H), 5.55 (m, 0.12H), 5.47 (d, $J = 7.6$ Hz, 0.8H), 5.29 (d, $J = 7.6$ Hz, 0.15H), 5.16 (t, $J = 7.2$ Hz, 0.96H), 5.07 (m, 0.92H), 4.12 (t, $J = 7.6$ Hz, 1H), 3.98 (m, 1H), 3.84 (m, 2H), 3.53, 3.54 (2 s, 5.8H), 3.31 (s, 0.2H), 3.11 (m, 1H), 2.36 (m, 1H), 2.17 (m, 2H), 2.08 (m, 1H), 1.97 (m, 3H), 1.83 (m, 1H), 0.92 (d, $J = 6.8$ Hz, 0.2H), 0.89 (d, $J = 6.8$ Hz, 0.2H), 0.83 (d, $J = 6.8$ Hz, 2.8H), 0.76 (d, $J = 6.8$ Hz, 2.8H). ESIHRMS m/z calcd for $C_{47}H_{47}FN_8O_6$ $[M+H]^+$ 839.3675; found 839.3665.

Methyl [(S)-1-((S)-2-{5-[4-(4-{2-[(S)-1-((R)-2-methoxycarbonylamino-2-phenyl-acetyl)-pyrrolidin-2-yl]-3H-imidazol-4-yl]-buta-1,3-dienyl)-3-phenoxy-phenyl]-1H-imidazol-2-yl)-pyrrolidine-1-carbonyl]-2-methyl-propyl]-carbamate dihydrochloride (1.22·2HCl, 28%): LC/MS 837 (M+H)⁺. ¹H NMR (DMSO-d₆, 400 MHz) δ 14.76 (brs, 0.6H), 8.19 (s, 1H), 7.95 (s, 1H), 7.86 (m, 1H), 7.79 (m, 1.4H), 7.66 (m, 0.8H), 7.59 (s, 0.8H), 7.59 (m, 0.2H), 7.42 (m, 2H), 7.34 (m, 4.4H), 7.24 (d, J = 8.0 Hz, 0.8H), 7.18 (t, J = 6.8 Hz, 1H), 7.12 (m, 0.4H), 7.06 (d, J = 8.0 Hz, 2H), 6.94 (m, 0.2H), 5.64 (m, 0.01H), 5.54 (m, 0.08H), 5.47 (d, J = 8.4 Hz, 0.79H), 5.29 (d, J = 7.6 Hz, 0.16H), 5.09 (m, 1.96H), 4.09 (t, J = 7.6 Hz, 1H), 3.92 (m, 1H), 3.83 (m, 3H), 3.52, 3.53 (2 s, 5.8H), 3.27 (s, 0.2H), 3.10 (m, 1H), 2.34 (m, 1H), 2.14 (m, 2H), 1.97 (m, 4H), 1.83 (m, 1H), 0.89 (d, J = 6.8 Hz, 0.2H), 0.86 (d, J = 6.8 Hz, 0.2H), 0.78 (d, J = 6.8 Hz, 2.8H), 0.73 (d, J = 6.8 Hz, 2.8H). ESIHRMS *m/z* calcd for C₄₇H₄₈N₈O₇ [M+H]⁺ 837.33718; found 837.3710.

Methyl [(S)-1-((S)-2-{5-[4-(4-{2-[(S)-1-((R)-2-methoxycarbonylamino-2-phenyl-acetyl)-pyrrolidin-2-yl]-3H-imidazol-4-yl]-buta-1,3-dienyl)-3-phensulphanyl-phenyl]-1H-imidazol-2-yl)-pyrrolidine-1-carbonyl]-2-methyl-propyl]-carbamate dihydrochloride (1.23·2HCl, 36%): LC/MS 853 (M+H)⁺. ¹H NMR (DMSO-d₆, 400 MHz) δ 15.38 (brs, 0.3H), 14.91 (brs, 0.6H), 8.12 (s, 1H), 8.05 (s, 0.9H), 7.95 (m, 2H), 7.87 (m, 1H), 7.79 (m, 0.1H), 7.68 (d, J = 7.6 Hz, 0.7H), 7.64 (m, 0.15H), 7.36 (m, 9.85H), 7.24 (d, J = 9.2 Hz, 0.8H), 7.14 (m, 0.35H), 6.98 (m, 0.15H), 5.69 (m, 0.05H), 5.60 (m, 0.1H), 5.48 (d, J = 7.6 Hz, 0.8H), 5.32 (d, J = 7.6 Hz, 0.15H), 5.13 (m, 1.9H), 4.10 (t, J = 7.6 Hz, 1H), 3.97 (m, 1H), 3.89 (m, 1H), 3.81 (m, 1H), 3.52, 3.53 (2 s, 5.85H), 3.27 (s, 0.15H), 3.11 (m, 1H), 2.34 (m, 1H), 2.16 (m, 2H), 2.06 (m, 1H), 1.97 (m, 3H), 1.84 (m, 1H), 0.90 (m, 0.4H), 0.79 (d, J = 6.8 Hz, 2.8H), 0.73 (d, J = 6.8 Hz, 2.8H). ESIHRMS *m/z* calcd for C₄₇H₄₈N₈O₆S [M+H]⁺ 853.3490; found 853.3477.

Methyl (S)-1-((S)-2-{5-[4-(4-{2-[(S)-1-((R)-2-methoxycarbonylamino-2-phenyl-acetyl)-pyrrolidin-2-yl]-3H-imidazol-4-yl]-buta-1,3-dienyl)-3-(methyl-phenyl-amino)-phenyl]-1H-imidazol-2-yl)-pyrrolidine-1-carbonyl]-2-methyl-propyl]-carbamate trihydrochloride (1.24·3HCl, 37%): LC/MS 850 (M+H)⁺. ¹H NMR (DMSO-d₆, 400 MHz) δ 15.21 (brs, 0.3H), 14.75 (brs, 0.6H), 8.22 (s, 1H), 7.89 (m, 0.8H), 7.85 (m, 1H), 7.76 (m, 2.1H), 7.65 (d, J = 7.6 Hz, 0.8H), 7.51 (m, 0.1H), 7.34 (m, 4.5H), 7.23 (m, 2.9H), 7.11 (m, 0.5H), 6.93 (m, 0.3H), 6.84 (t, J = 7.6 Hz, 1H), 6.77 (d, J = 8.0 Hz, 2H), 5.67 (m, 0.05H), 5.52 (m, 0.1H), 5.47 (d, J = 7.6 Hz, 0.8H), 5.29 (d, J = 7.6 Hz, 0.15H), 5.14 (t, J = 6.8 Hz, 1H), 5.06 (m, 0.9H), 4.10 (t, J = 7.6 Hz, 1H), 3.94 (m, 1H), 3.84 (m, 2H), 3.52, 3.53 (2 s, 5.8H), 3.35 (s, 3H), 3.31 (s, 0.2H), 3.10 (m, 1H), 2.35 (m, 1H), 1.89–2.20 (m, 6H), 1.82 (m, 1H), 0.90 (m, 0.4H), 0.81 (d, J = 6.8 Hz, 2.8H), 0.75 (d, J = 6.8 Hz, 2.8H). ESIHRMS *m/z* calcd for C₄₈H₅₁N₉O₆ [M+H]⁺ 850.4035; found 850.4033.

5.2. Molecular modeling

Ligands and protein preparation, homology modeling, docking simulations were performed using the Maestro suite (release 2015-2).²⁹ The homodimeric structure of HCV NS5A gT3a was constructed exploiting Structure Prediction Wizard implemented in Prime. The protein sequence of the N-terminal region (residues 1–198) was extracted from the NCBI Protein database (access code AFP27699.1). The mode-II structure of D-I attached to the terminal alpha-helices described by Nettles et al.²⁷ was applied as a template for homology modeling. Both subunits were reconstructed simultaneously using a knowledge-based method for a homo-multimer model type. Zn²⁺ cations in the area of zinc-fingers and the ligand were included during the model construction. The obtained protein structure was preprocessed with the Protein Preparation Wizard tool at the following settings: amino acid residue state generation (Epik, at pH = 7.4 ± 0) and restrained minimization (converge heavy atoms to RMSD 0.8 Å). After preprocessing the flexible linker (residues 28–36) of chain A had been refined, exploiting the Refine Loops tool implemented in Prime. The refinement was performed with an extended serial loop sampling method, recommended for loops with 6–11 residues. Side chains were refined within 4.5 Å. It resulted in ten models. For each of them, the same region of chain B was

refined as well. Finally, ten sets with ten structures in each one were obtained. From each set, a model with the lowest potential energy was selected for further assessment. Receptor Grid Generation tool was used to generate a grid for the following docking procedures. Coordinates of the center of the grid: X = 5.74, Y = 10.24, Z = 53.34. Box size: length X = 17, box length Y = 10, box length Z = 17.

2D structures of ligands were preprocessed using the LigPrep tool at default settings. Chiralities were specified prior to preprocessing and inspected manually after conformers generation. Docking simulations were performed with the Ligand Docking tool (Glide) at standard precision mode. Obtained conformers were sorted by the values of the Glide Emodel score function and inspected manually.

5.3. Replicon antiviral assay

The human hepatoma cell line Huh7 harboring the HCV replicon was used as the test line to perform the assay. Compounds were tested for their inhibitory activities in the HCV gT1a, gT1b, gT2a, gT3a, gT4a, gT5a subgenomic replicons assays with the addition of 10% FBS. Cells were seeded at a density of 3 × 10³ cells per well in 384-well plates containing 40 µL of assay media (DMEM 1 ×, Cellgro, catalogue no. 10-013-CV). After overnight incubation of the cells at 37 °C in a 5% CO₂ atmosphere compound treatment was initiated. A total of 10 serial 3.16-fold dilutions of the test compounds were prepared as 200 × stock in DMSO. Then 5 × compounds solution was prepared fresh in the assay medium and 10 µL of this 5 × solution was transferred to the plates with cells. The final concentration of the compounds was from 10 nM to 0.1 pM. The final DMSO concentration was 0.5%. Test examples were then incubated for 3 days at 37 °C in a 5% CO₂ atmosphere. Bright-Glo reagent (25 ml) was added in each well of assay plates after 72 h of incubation with compounds. Intensity of luminescence were measured for each well on the Victor Light luminescence counter after 3–5 min of incubation with Bright-Glo reagent.

5.4. Cytotoxicity

Cytotoxicity of the tested compounds was evaluated in parallel using the same human hepatoma cell line Huh7 in gT1b replicon by analogy to the procedure described above. CellTiter-Glo reagent (10 ml) was used instead of Bright-Glo reagent after 72 h of incubation with the test compound. Intensity of luminescence was measured for each well using Victor Light luminescence counter after 3–5 min of incubation. All the compounds showed an CC₅₀ value over 10 µM.

5.5. PK study in rats

Animal studies were carried out following protocols approved by the Institutional Animal Care and Use Committees as well as institutional guidelines for the proper, humane use of animals in research. Male Sprague-Dawley rats (8–10 weeks) obtained from Charles River Laboratories International, Inc., Germany were used for PK studies. Animals were housed under controlled conditions (22–26 °C, relative humidity 30–70%) with a natural light/dark cycle (12 h/12 h). Animals were previously catheterized in the jugular vein and fasted for 12 h before the study with free access to water. Compounds were dissolved in 10% DMSO/10% Solutol/80% 0.05 M N-methylglucamine for IV administration (5 ml/kg) and in 0.5% methyl cellulose for PO administration (10 ml/kg). Blood samples were taken in EDTA-containing tubes 5, 15, 30 min, 1, 2, 4, 8 and 24 h after IV administration and 15, 30 min, 1, 2, 4, 8 and 24 h after oral administration. Plasma samples (45 µL) were prepared by centrifugation of the blood, mixed with 5 µL of acetonitrile:H₂O (1:1 v/v) and precipitated with 150 µL of acetonitrile containing the internal standard tolbutamide (50 ng/mL). Samples were incubated at –20 °C for 15 min followed by centrifugation at 11,000 g for 10 min, and then the supernatants (130 µL) were transferred into a new plate for LC-MS/MS analysis. The analysis was

performed using Agilent 1290 UPLC coupled with Qtrap5500 mass spectrometer (ABSciex, USA). PK parameters were calculated using noncompartmental analysis provided by the software WinNonlin Professional 5.2 (Pharsight Corporation).

Author contributions

The manuscript was written through contributions of all authors. All authors have given approval to the final version of the manuscript.

Funding

The authors also acknowledge the financial support of Russian Science Foundation [grant number 17-74-30012], IBG RAS Ufa (*in silico* study).

Declaration of Competing Interest

The authors declare that they have no known competing financial interests or personal relationships that could have appeared to influence the work reported in this paper.

Acknowledgements

The authors gratefully thank Alexandre V. Ponomarev, Dr. Yulia A. Pelogeykina, Ekaterina Yu. Volosova for excellent technical assistance.

Appendix A. Supplementary material

Supplementary data to this article can be found online at <https://doi.org/10.1016/j.bmc.2020.115716>.

References

- Choo Q, Kuo G, Weiner A, Overby L, Bradley D, Houghton M. Isolation of a cDNA clone derived from a blood-borne non-A, non-B viral hepatitis genome. *Science*. 1989;244:359–362. <https://doi.org/10.1126/science.2523562>.
- Kuo G, Choo Q-L, Alter HJ, et al. An assay for circulating antibodies to a major etiologic virus of human non-A, non-B hepatitis. *Science*. 1989;244:362–364. <https://doi.org/10.1126/science.2496467>.
- Polaris Observatory HCV Collaborators, Collaborators (222), Blach S, et al. Global prevalence and genotype distribution of hepatitis C virus infection in 2015: a modelling study. *Lancet Gastroenterol Hepatol*. 2017;2:161–176. [https://doi.org/10.1016/S2468-1253\(16\)30181-9](https://doi.org/10.1016/S2468-1253(16)30181-9).
- WHO. Hepatitis C; 2019. <https://www.who.int/news-room/fact-sheets/detail/hepatitis-c> [accessed 13 December 2019].
- Hedskog C, Parhy B, Chang S, et al. Identification of 19 novel hepatitis C Virus subtypes—further expanding HCV classification. *Open Forum Infect. Dis*. 2019;6:ofz076. <https://doi.org/10.1093/ofid/ofz076>.
- Spach DH, Kim HN. Treatment of HCV genotype 1. Hepatitis C online 2019, Sec. 5, Top. 3; 2019. <https://www.hepatitisc.uw.edu/go/treatment-infection/treatment-genotype-1/core-concept/all> [accessed 16 January 2020].
- Spach DH, Kim HN. Treatment of HCV genotype 1. Hepatitis C online 2019, Sec. 5, Top. 2; 2019. <https://www.hepatitisc.uw.edu/go/treatment-infection/treatment-genotype-2/core-concept/all#introduction> [accessed 16 January 2020].
- Spach DH, Kim HN. Treatment of HCV genotype 3. Hepatitis C online 2019, Sec. 5, Top. 3; 2019. <https://www.hepatitisc.uw.edu/go/treatment-infection/treatment-genotype-3/core-concept/all> [accessed 16 January 2020].
- Chan A, Patel K, Naggie S. Genotype 3 infection: the last stand of hepatitis C virus. *Drugs*. 2017;77:131–144. <https://doi.org/10.1007/s40265-016-0685-x>.
- Spach DH, Kim HN. Treatment of HCV genotype 4. Hepatitis C online 2019, Sec. 5, Top. 4; 2019. <https://www.hepatitisc.uw.edu/go/treatment-infection/treatment-genotype-4/core-concept/all> [accessed 16 January 2020].
- Spach DH, Kim HN. Treatment of HCV genotype 5 or 6. Hepatitis C online 2019, Sec. 5, Top. 5 or 6; 2019. <https://www.hepatitisc.uw.edu/go/treatment-infection/treatment-genotype-5-or-6/core-concept/all> [accessed 16 January 2020].
- Belda O, Targett-Adams P. Small molecule inhibitors of the hepatitis C virus-encoded NS5A protein. *Virus Res*. 2012;170:1–14. <https://doi.org/10.1016/j.virusres.2012.09.007>.
- Nettles JH, Jenkins JL, Bender A, Deng Z, Davies JW, Glick M. Asymmetric binding to NS5A by daclatasvir (BMS-790052) and analogs suggests two novel modes of HCV inhibition. *J Med Chem*. 2006;49:6802–6810. <https://doi.org/10.1021/jm501291c>.
- Belema M, Lopez OD, Bender JA, et al. Discovery and development of hepatitis C virus NS5A replication complex inhibitors. *J Med Chem*. 2014;57:1643–1672. <https://doi.org/10.1021/jm401793m>.
- Nitta S, Asahina Y, Matsuda M, et al. Effects of resistance-associated NS5A mutations in hepatitis C virus on viral production and susceptibility to antiviral reagents. *Sci Rep*. 2016;6:34652. <https://doi.org/10.1038/srep34652>.
- Coburn CA, Meinke PT, Chang W, et al. Discovery of MK-8742: an HCV NS5A inhibitor with broad genotype activity. *Chem Med Chem*. 2013;8:1930–1940. <https://doi.org/10.1002/cmdc.201300343>.
- Link JO, Taylor JG, Xu L, et al. Discovery of ledipasvir (GS-5885): a potent, once-daily oral NS5A inhibitor for the treatment of hepatitis C virus infection. *J Med Chem*. 2014;57:2033–2046. <https://doi.org/10.1021/jm401499g>.
- Ivachtchenko AV, Mitkin OD, Yamanushkin PM, et al. Discovery of novel highly potent hepatitis C virus NS5A inhibitor (AV4025). *J Med Chem*. 2014;57:7716–7730. <https://doi.org/10.1021/jm500951r>.
- DeGoey DA, Randolph JT, Liu D, et al. Discovery of ABT-267, a pan-genotypic inhibitor of HCV NS5A. *J Med Chem*. 2014;57:2047–2057. <https://doi.org/10.1021/jm401398x>.
- Vince B, Hill JM, Lawitz EJ, et al. A randomized, double-blind, multiple-dose study of the pan-genotypic NS5A inhibitor samatasvir in patients infected with hepatitis C virus genotype 1, 2, 3 or 4. *J Hepatol*. 2014;60:920–927. <https://doi.org/10.1016/j.jhep.2014.01.003>.
- Bilello JP, Lalloos LB, McCarville JF, et al. In vitro activity and resistance profile of samatasvir, a novel NS5A replication inhibitor of hepatitis C virus. *Antimicrobial Agents Chemother*. 2014;58:4431–4442. <https://doi.org/10.1128/AAC.02777-13>.
- Tong L, Yu W, Chen L, et al. Discovery of ruzasvir (MK-8408): a potent, pan-genotypic HCV NS5A inhibitor with optimized activity against common resistance-associated polymorphisms. *J Med Chem*. 2017;60:290–306. <https://doi.org/10.1021/acs.jmedchem.6b01310>.
- Yu W, Hu B, Zhong B, et al. Discovery of novel pan-genotypic HCV NS5A inhibitors containing a novel tetracyclic core. *Bioorg Med Chem Lett*. 2019;29:700–706. <https://doi.org/10.1016/j.bmcl.2019.01.031>.
- Yu W, Tong L, Selyutin O, et al. Discovery of MK-6169, a potent pan-genotype hepatitis C virus NS5A inhibitor with optimized activity against common resistance-associated substitutions. *J Med Chem*. 2018;61:3984–4003. <https://doi.org/10.1021/acs.jmedchem.7b01927>.
- Wagner R, Randolph JT, Patel SV, et al. Highlights of the structure–activity relationships of benzimidazole linked pyrrolidines leading to the discovery of the hepatitis C virus NS5A inhibitor pibrentasvir (ABT-530). *J Med Chem*. 2018;61:4052–4066. <https://doi.org/10.1021/acs.jmedchem.8b00082>.
- Ivanenkov YA, Veselov MS, Shakhbazyan AG, et al. A comprehensive insight into the chemical space and ADME features of small molecule NS5A inhibitors. *Curr Top Med Chem*. 2016;16:1372–1382. <https://doi.org/10.2174/1568026616666151120113040>.
- Nettles JH, Stanton RA, Brody J, et al. Asymmetric binding to NS5A by daclatasvir (BMS-790052) and analogs suggests two novel modes of HCV inhibition. *J Med Chem*. 2014;57. <https://doi.org/10.1021/jm501291c>.
- Knops E, Sierra S, Kalaghatgi P, Heger E, Kaiser R, Kalinina OV. Epistatic interactions in NS5A of hepatitis C virus suggest drug resistance mechanisms. *Genes*. 2018;9(7):343. <https://doi.org/10.3390/genes9070343>.
- Schrödinger Suite software: Maestro, Schrödinger, LLC, New York, NY; 2019. <https://www.schrodinger.com> [accessed 16 January 2020].
- Ahmed M, Pal A, Houghton M, Barakat KA. Comprehensive computational analysis for the binding modes of hepatitis C virus NS5A inhibitors: the question of symmetry. *ACS Infect Dis*. 2016;2:872–881. <https://doi.org/10.1021/acsinfecdis.6b00113>.
- Belema M, Meanwell NA. Discovery of daclatasvir, a pan-genotypic hepatitis C virus NS5A replication complex inhibitor with potent clinical effect. *J Med Chem*. 2014;57(12):5057–5071. <https://doi.org/10.1021/jm500335h>.
- Li L, Zhong M. Inhibitors of HCV NS5A. *Intern. Pat. Appl*. 2010 WO 2010/065668.
- Vandyck K, Last SJ, Houppis IN, Raboisson PJ-MB. Benzimidazole-imidazole derivatives. *Intern. Pat. Appl*. 2011 WO 2011054834.
- Romine JL, Belema DR St, Laurent M, et al. Hepatitis C virus inhibitors. *Intern. Pat. Appl*. 2010 WO 2010096302.